# Waves upstream and downstream of interplanetary shocks driven by coronal mass ejections

P. Kajdič,[1] X. Blanco-Cano,[1] E. Aguilar-Rodriguez,[2] C. T. Russell,[3] L. K. Jian,[3] and J. G. Luhmann[4]

Received 16 November 2011; revised 13 April 2012; accepted 25 April 2012; published 8 June 2012.

[1] In this work we study the waves in regions adjacent to ten interplanetary (IP) shocks formed by the interactions between interplanetary coronal mass ejections and the solar wind. We analyze the STEREO data for the years 2007–2010. Shocks in our sample have low magnetosonic Mach numbers ($M_{ms} \leq 2.3$), their criticality ratios range between 0.8 and 2.3 and $\theta_{Bn}$ are between 38° and 85°. We find ultra-low frequency (ULF, 0.01 Hz–0.05 Hz) waves and higher-frequency (HF, ≥ 1 Hz) whistler precursors upstream of these shocks. Downstream of them we observe irregular ULF fluctuations and regular HF waves with similar frequencies as in the upstream case. We find that IP shocks with relatively small $M_{ms}$ can excite waves in large regions in front of them ($2.2 \times 10^{-3}$ AU–$4.6 \times 10^{-3}$ AU), thereby forming large ULF wave foreshocks. We do not find any evidence for the steepening of these waves. We do observe suprathermal (E ≤ 30 keV) proton foreshocks upstream of some of the shocks in the sample. The extensions of suprathermal proton foreshocks range between 0.02 AU and 0.1 AU. However, not all foreshocks with suprathermal ions show ULF waves or vice versa. The extensions of ULF and proton foreshocks can be very different. Enhanced ULF waves and suprathermal protons can be observed upstream of local quasi-perpendicular shocks. We propose that the observed discordance between the shock geometries and the presence of the foreshock phenomena may be explained in terms of temporal and spatial variations of the local geometry of the IP shocks.

**Citation:** Kajdič, P., X. Blanco-Cano, E. Aguilar-Rodriguez, C. T. Russell, L. K. Jian, and J. G. Luhmann (2012), Waves upstream and downstream of interplanetary shocks driven by coronal mass ejections, *J. Geophys. Res.*, *117*, A06103, doi:10.1029/2011JA017381.

## 1. Introduction

[2] It has long been known that waves can appear in the regions upstream and downstream of collisionless shocks [see, e.g., *Farris et al.*, 1993; *Blanco-Cano*, 2010]. Observational studies [*Fairfield*, 1969, 1974; *Russell et al.*, 1971, 1983; *Hoppe et al.*, 1982; *Tsurutani et al.*, 1983] revealed that various types of waves can exist upstream of such shocks. The most common types are the ultra-low frequency (ULF) and whistler waves.

[3] Whistler waves were first observed upstream of the Earth's bow shock by *Heppner et al.* [1967] and *Russell et al.* [1971]. In general it was recognized that the whistlers are formed at the shocks and then they propagate upstream [*Fairfield*, 1974; *Greenstadt et al.*, 1981; *Orlowski et al.*, 1995]. *Feldman et al.* [1983] and *Orlowski et al.* [1995] showed that, in the case of the Earth's bow shock, there is a connection between the whistlers and the backstreaming electrons in the intermediate energy range between 15 eV and 45 eV. Similar conclusions were reached about the whistler waves observed upstream of IP shocks [*Tsurutani et al.*, 1983] and of bow shocks around Mercury, Venus and Saturn [*Orlowski et al.*, 1990, 1992; *Orlowski and Russell*, 1991, 1995; *Russell*, 2007]. The whistler waves may be observed as phase-standing waves that propagate parallel to the local shock normal, as obliquely propagating upstream whistler precursors and as wave packets adjacent to the steepened edges of shocklets. *Wilson et al.* [2009] observed whistler waves and shocklets at five quasi-perpendicular interplanetay shocks. Four of these shocks had non phase-standing whistler precursors just upstream of them. The authors find that the observed whistlers were associated with electron distributions that are unstable to whistler heat flux

[1]Instituto de Geofísica, Universidad Nacional Autónoma de México, Ciudad Universitaria, Mexico City, Mexico.
[2]Instituto de Geofísica, Unidad Michoacán, Universidad Nacional Autónoma de México, Morelia, Mexico.
[3]Institute of Geophysics and Planetary Physics, University of California, Los Angeles, California, USA.
[4]Space Sciences Laboratory, University of California, Berkeley, California, USA.

Corresponding author: P. Kajdič, Institudo de Geofisica, Universidad Nacional Autónoma de México, Ciudad Universitaria, Mexico City, DF 04510, Mexico. (primoz@geofisica.unam.mx)

**Table 1.** Properties of ICMEs in Our Sample

| ICME Start (UT) | ICME End (UT) | Spacecraft STEREO | $V_{SW}$ (km s$^{-1}$) | $V_{ICME}$ (km s$^{-1}$) | ICME Type |
|---|---|---|---|---|---|
| Jun 7, 2010 22:21 | Jun 8, 2010 12:30 | B | 330 | 360 | |
| Apr 23, 2010 06:27 | Apr 23, 2010 14:06 | A | 370 | 420 | MC |
| Jun 19, 2009 07:40 | Jun 20, 2009 10:00 | B | 280 | 380 | MC |
| Jan 25, 2009 18:22 | Jan 27, 2009 10:00 | A | 350 | 410 | MC |
| Nov 20, 2010 06:34 | Nov 21, 2010 09:10 | B | 420 | 500 | MC |
| Apr 29, 2008 15:34 | Apr 30, 2007 07:00 | B | 410 | 600 | MC |
| Aug 6, 2009 04:39 | Aug 7, 2009 05:24 | B | 360 | 550 | MC |
| Jul 5, 2008 06:34 | Jul 7, 2008 18:00 | A | 290 | 400 | MC |
| Oct 16, 2009 21:35 | Oct 17, 2009 22:16 | A | 300 | 400 | MC |
| Oct 3, 2009 05:48 | Oct 4, 2009 04:32 | B | 260 | 350 | MC |

and/or whistler anisotropy instabilities. They explain the origin of the waves in terms of these instabilities.

[4] Another type of fluctuations are the ULF fluctuations which may appear as 0.01–0.05 Hz transverse, large-amplitude, elliptically polarized waves or as linearly polarized ULF fluctuations. In the case of planetary bow shocks, the ULF waves may further steepen into shocklets [*Hoppe et al.*, 1981; *Hoppe and Russell*, 1983] and short large-amplitude magnetic structures (SLAMS) [see, e.g., *Schwartz and Burgess*, 1991; *Schwartz*, 1991; *Schwartz et al.*, 1992; *Giacalone et al.*, 1993; *Scholer*, 1993].

[5] Theoretical studies [*Biskamp*, 1973] also predict downstream standing waves but only for nearly perpendicular low-Mach number shocks ($\theta_{Bn} > 88.5°$). In contrast to the theoretical predictions, wave trains were observed downstream of low-Mach number, low-$\beta$, quasi-perpendicular shocks near Venus [*Balikhin et al.*, 2008]. This was explained in terms of kinematic relaxation [*Ofman et al.*, 2009].

[6] Recently *Russell et al.* [2009] performed a study of 60 IP low-Mach number shocks observed by STEREO. Most of the shocks studied in this work were driven by stream interactions. Waves in the upstream and downstream regions of the shocks were observed for a wide range of interplanetary conditions.

[7] Collisionless shocks in the solar wind (SW) occur when fast interplanetary coronal mass ejections (ICMEs) interact with the ambient SW or when fast streams of solar wind plasma overtake the slow ones. If the difference in speeds between the two interacting plasmas is large enough (super-magnetosonic), the interplanetary (IP) shocks form. Energetic particles and ULF perturbations of the interplanetary magnetic field (IMF) are often detected several hours before the shocks. In the past most studies focused on the macro-structure of transient shocks, while less attention was given to their micro-structure and the wave-particle phenomena associated with them (see *Blanco-Cano* [2010] for a review on shocks in the SW). Little is known about the properties of the waves that populate regions adjacent to the shock transitions and there are still open questions about how much steepening of the ULF waves occurs at IP shocks and how extended the regions of suprathermal ions are.

[8] In this work we perform a survey of ICME driven IP shocks observed by STEREO spacecraft during the years 2007–2010 in order to study the waves that appear in their upstream and downstream regions. We focus on the effects that the ICME driven shocks have on the ambient SW. We study the waves around shocks formed due to the interaction between the ICMEs and the solar wind plasma. Ten shocks satisfying the selection criteria were found. We use STEREO B-field data at high resolution (8 Hz and 32 Hz) and plasma data at 1-minute time resolution.

[9] This paper is organized as follows: in section 2 we present our event sample and discuss three shocks in detail. In section 3 we discuss the results, in section 4 we present the conclusions and in section 5 we summarize our results.

## 2. Observations

[10] The list of all ICMEs and IP shocks observed by the STEREO spacecraft is available at the STEREO Web page (http://wwwssc.igpp.ucla.edu/forms/stereo/stereo_level_3.html). In order to study IP shocks and the adjacent regions, we use the magnetic field data provided by the IMPACT instrument [*Luhmann et al.*, 2008a, 2008b] and the plasma data provided by the PLASTIC instrument [*Galvin et al.*, 2008]. The B-field data are available in three modes—in the continuous modes with 1 Hz and 8 Hz time resolutions and in the burst mode with 32 Hz resolution. The data in 32 Hz resolution are available only for short, selected time intervals. The PLASTIC instrument operates with 1 minute time resolution, providing measurements of solar wind moments.

[11] During the years 2007–2010 the STEREO spacecraft observed ten ICMEs with IP shocks. We present their properties in Table 1. The columns of the table provide the following data: (1) the date and time at which the ICME was first detected, (2) the date and time at which the ICME ended, (3) the STEREO spacecraft (A or B) that observed the ICME (the November 19, 2007 ICME was observed by both spacecraft, but its shock was observed only by STEREO B), (4) the average SW speed during a five minute time interval prior to the associated IP shock, (5) the maximum velocity of the ICME and (6) the type of ICME if it could be determined (MC stands for magnetic cloud). The criteria used to determine if the ICME was a MC were: (1) the B-field magnitude inside a CME had to be larger than in the unperturbed SW, (2) the plasma beta had to be lower than in the surrounding SW and (3) smooth rotations of the B-field components had to be present inside the event.

[12] Table 2 provides information on the shocks and associated usptream/downstream regions. In this table we provide (1) the date of the IP shocks, (2) the time at which they were detected, (3) the information on 32 Hz data availability, (4) the angle between the upstream IMF and the shock normal, $\theta_{Bn}$ (the shocks are listed in order of descending $\theta_{Bn}$), (5) the angle between the shock normal and the radial direction, $\theta_{nR}$, (6) the shock's magnetosonic Mach number ($M_{ms}$), (7) the ratio between the shock's $M_{ms}$ number and the critical Mach number (calculated with the XSPACE

**Table 2.** ICME Driven IP Shocks Observed Between the Years 2007 and 2010

| Date | Time (UT) | 32 Hz Data | $\theta_{Bn}$ (deg) | $\theta_{nR}$ (deg) | $M_{ms}$ | Criticality Ratio | $\beta_{up}$ | ULF Waves Up | ULF Waves Down | HF Waves Up | HF Waves Down | ULF Foreshock Size ($10^{-3}$ AU) | HF Foreshock Size ($10^{-3}$ AU) | Suprathermal Ions (AU) |
|---|---|---|---|---|---|---|---|---|---|---|---|---|---|---|
| Jun 7, 2010 | 04:08:50 | y | 85 | 33 | 1.7 | 1.7 | 3.2 | n | y | y | y | | 0.002 | 0.04 |
| Apr 23, 2010 | 00:34:37 | n | 77 | 83 | 1.3 | 1.1 | 2.8 | n | n | y | y | 2.5 | | 0.10 |
| Jun 19, 2009 | 00:23:34 | y | 77 | 12 | 1.9 | 1.6 | 5.9 | n | n | n | y | | | 0.02 |
| Jan 25, 2009 | 18:22:52 | y | 76 | 45 | 1.5 | 1.2 | 3.1 | n | n | n | n | | | |
| Nov 19, 2010 | 20:26:00 | n | 72 | 81 | 1.5 | 1.1 | 1.7 | n | y | y | y | | 0.10 | |
| Apr 29, 2008 | 14:10:08 | n | 68 | 16 | 1.8 | 1.1 | 1.0 | n | n | y | n | | 0.13 | 0.06 |
| Aug 5, 2009 | 22:35:20 | y | 54 | 30 | 1.7 | 1.5 | 4.4 | y | y | y | n | 4.6 | 0.11 | |
| Jul 5, 2008 | 00:47:54 | y | 52 | 60 | 1.7 | 1.3 | 2.1 | n | n | y | n | | 0.22 | |
| Oct 16, 2009 | 14:56:55 | y | 48 | 34 | 1.2 | 0.8 | 0.9 | n | n | n | n | | | |
| Oct 2, 2009 | 15:43 50 | y | 38 | 17 | 2.3 | 2.3 | 16.5 | y | y | y | n | 2.2 | 0.02 | 0.06 |

program, available at the UCLA IGPP Web page, http://www-ssc.igpp.ucla.edu/ssc/software/xspace.html), (8) the upstream betas, (9) through (12) the information on whether enhanced ULF or high-frequency (HF) waves appear upstream or downstream of the shocks, (13) the extent of the region upstream with enhanced ULF waves as observed by the spacecraft and (14) the extent of the region of enhanced HF waves, (15) the extent of the suprathermal (E > 1 keV) protons foreshock in the data of the PLASTIC instrument. The PLASTIC data are available on the Web page http://fiji.sr.unh.edu/cgi-bin/wap_bfield_public.cgi/.

[13] In order to obtain $\theta_{Bn}$ and $\theta_{nR}$, we use the STEREO Magnetometer Data to calculate the orientation of the shock's normal in the RTN system by using the coplanarity theorem. We also calculate the average plasma properties upstream and downstream of the shocks (SW velocity, $\beta$, T and n). We then calculate the shock's $M_{ms}$ and the ratio of criticality with the XSPACE program (C. T. Russell et al., Educational software for the visualization of space plasma processes, 1999, available at http://www-ssc.igpp.ucla.edu/ssc/spgroup_edu.html).

[14] Three shocks are presented here in detail as case studies. These were observed on August 5, 2009 (Figure 2), June 19, 2009 (Figure 7), and October 2, 2009 (Figure 10). The first two are quasi-perpendicular shocks ($\theta_{Bn} > 45°$), while the latter is a quasi-parallel IP shock.

### 2.1. Case Studies

[15] In this section we present three ICMEs and their associated shocks. These events were chosen for the following reasons: the shock observed on August 5, 2009 is quasi-perpendicular ($\theta_{Bn} = 54°$), but there is an extended ULF wave foreshock upstream of it, which, in the case of the Earth's bow shock, is a characteristic of quasi-parallel geometries. Also, no suprathermal protons are associated with this foreshock, which is unexpected, since in the case of the Earth's bow shock, the ULF wave and the suprathermal ion foreshocks coincide almost completely. The shock observed on June 19, 2009 exhibits regular downstream fluctuations similar to those discovered by *Balikhin et al.* [2008] in the bow-shock of Venus. In the case of IP shocks these fluctuations have been observed only by *Russell et al.* [2009] for SIR driven shocks. Finally, the October 2, 2009 event is the only quasi-parallel shock in our sample, with large ULF wave and suprathermal proton foreshocks.

[16] The B-field and SW velocity measured by STEREO at the time of each event are presented in Figure 1. The dashed vertical lines in all panels delimit the ICME's flux ropes and the dash-dotted vertical lines mark the times of the shocks.

[17] The first ICME (Figure 1a) was observed between August 6 4:39 UT and August 7 5:24 UT, 2009 by STEREO B. The preceding pristine SW velocity was 360 km $s^{-1}$ and the maximum velocity of the ICME was 550 km $s^{-1}$. This ICME was classified as a MC due to the smooth rotation of the B-field components, the enhanced magnetic field magnitude and low plasma beta (not shown here). The duration of the shock sheath region transit through the spacecraft was ~6 hours.

[18] The second is an ICME which was observed between June 19 7:40 UT and June 20 10:00 UT, 2009 by STEREO B (Figure 1b). The velocity of the SW prior to the arrival of the associated shock was 280 km $s^{-1}$, while the maximum velocity of the ICME was 380 $kms^{-1}$. Again, the ICME exhibits smooth B-field rotations, enhanced magnetic field magnitude and low plasma beta, and is therefore classified as a MC. The shock sheath region was observed during 5 hours.

[19] Figure 1c shows an ICME observed by STEREO B during October 03 05:48 UT, 2009 and Oct 04, 04:32 UT, 2009. The plasma velocity prior to the ICME driven IP shock was 260 km $s^{-1}$ and the maximum velocity of the ICME was 350 km $s^{-1}$. This ICME was also a MC. The shock sheath region was observed for ~10 hours.

[20] All three shock sheath regions are characterized by large fluctuations of magnetic field, including large-amplitude rotations of the field.

[21] In the following sections we present the shocks associated with these ICMEs and their adjacent regions. The magnetic field data are presented in the corresponding shock-normal coordinate system. In this system the $B_n$ component of the B-field points along the shock normal, $B_l$ is parallel to the projection of the upstream IMF onto the plane of the shock and $B_m$ completes the right-hand system.

[22] The advantage of presenting the shock transition in the shock-normal coordinate system is that one can see the Rankine-Hugoniot relations being satisfied at the shock—the average $B_n$ component of the B-field does not change across the shock, although small oscillations are still present. The $B_l$ changes in almost the same manner as the B-field intensity and the $B_m$ oscillates around zero. Also, in this system it is easier to recognize standing whistler precursors that are sometimes observed upstream of the low-Mach number, low-beta shocks [see, e.g., *Fairfield and Feldman*, 1975]. These waves only appear in $B_l$ and $B_m$

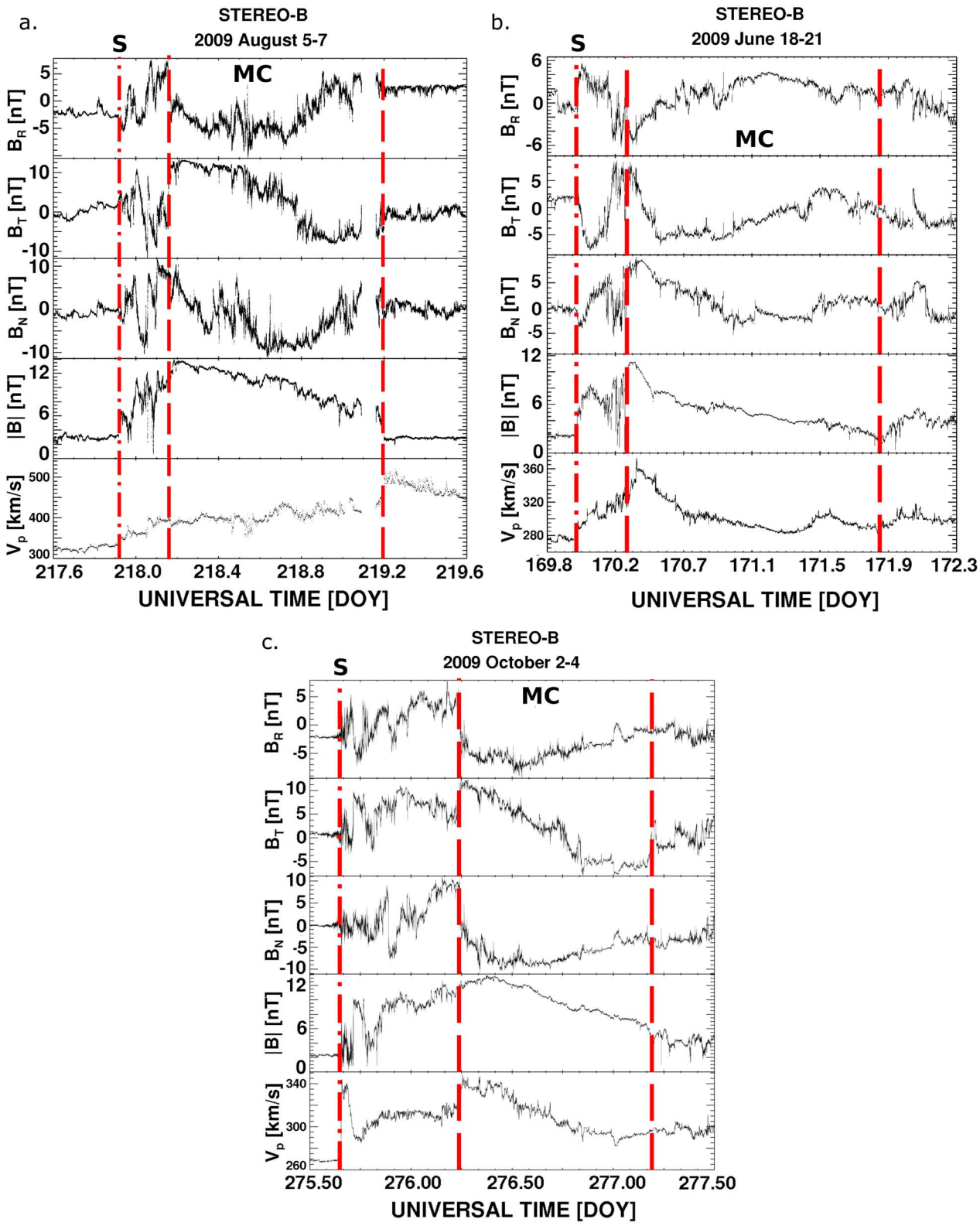


**Figure 1.** ICMEs in the B-field and SW velocity data of STEREO spacecraft observed between (a) August 5–August 7, 2009, (b) June 19–June 20, 2009 and (c) October 2–October 4, 2009. The vertical dashed lines mark the beginning and the end of the MCs. The vertical dashed-dotted line and the letter S mark the times of the shocks. MC stands for magnetic clouds and marks the flux ropes of the ICMEs.

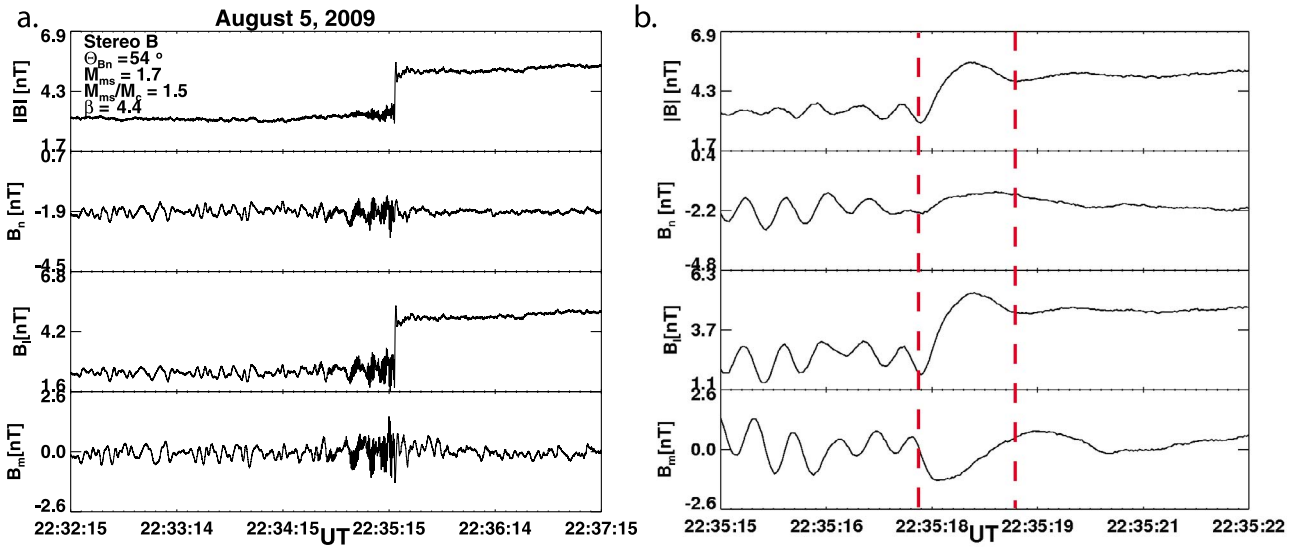


**Figure 2.** The IP shock observed on August 5, 2009. 32 Hz data is used. (a) Four minute time interval including the shock and the adjacent regions. (b) Closeup of the shock.

components of the B-field and propagate along the shock normal ($\theta_{nk} \sim 0°$). They are circularly polarized and their periods range from 6 to 130 s.

### 2.1.1. August 5, 2009 Event

[23] Figure 2a shows the IP shock observed on August 5, 2008 at 22:35:20 UT by STEREO B. Magnetic field data with 32 Hz time resolution is presented in the figure. This is a quasi-perpendicular ($\theta_{Bn} = 54°$), supercritical ($M_{ms}/M_c = 1.5$) shock with $M_{ms}$ = 1.7. The ratio $B_{down}/B_{up}$ = 2 and the upstream beta is 4.4. The magnitude of the field on the top panel on Figure 2a shows a sharp quasi-perpendicular shock profile. The shock transition is preceded by HF whistler waves that extend ~42 seconds upstream of the shock. The precursors are followed by a steep ramp and a pronounced overshoot in the B-field magnitude that is ~0.4 nT (~7.7%) higher than that in the downstream region.

[24] The shock transition is shown in detail in Figure 2b, where it is delimited by dashed vertical lines. The shock transition (the ramp and the overshoot) is best seen in the upper panel showing the B-field intensity and in the third panel from the top, showing the $B_l$ component. The ramp and the overshoot lasted for 1.4 seconds. Such a short duration of ICME driven IP shocks in the spacecraft data is due to their fast propagation across the spacecraft. The high-resolution 32 Hz B-field data allow us to study the structure of such shocks in more detail than ever before.

[25] An interval upstream of the shock is presented in Figure 3a. The three panels with the B-field components show a highly perturbed upstream region, which is unexpected and more typical of quasi-parallel shocks. There are two type of fluctuations present in the region—the longer wavelength, ULF fluctuations that populate the entire time interval and the HF, low-amplitude whistler waves that extend ~42 seconds upstream of the shock.

[26] Figure 3b shows a Fourier spectra of a portion of the upstream region close to the shock. There are two distinct peaks in the spectrum. A broad peak that extends between the frequencies of ~0.05 Hz (periods ~20 s) and ~0.4 Hz (2.5 s) belongs to the ULF waves. It can be seen that these waves exhibit mainly a transverse component. Hodograms in Figure 3c show that these ULF waves are left-hand (LH) circularly polarized in the spacecraft frame. The red +an ×signs mark the beginning and the end of the time series, respectively. The ratio between the intermediate and minimum variance (Int/Min) is 73 indicating planar waves. They propagate at an average $\theta_{Bk} \sim 2°$ with respect to the average upstream IMF.

[27] Figure 4a displays spectra of the upstream ULF waves during successive 10-minutes intervals obtained with the 8 Hz data (only the spectra of the transverse component are shown). The peak indicating the enhanced ULF wave activity is present for times up to ~30 minutes upstream of the shock. By multiplying this time interval with the upstream SW speed (380 km $s^{-1}$) we obtain a proxy of the size of this region along the spacecraft's trajectory to be $4.6 \times 10^{-3}$ AU. Although the calculated extensions are influenced by the way the spacecraft passed through the foreshock, this case still shows that even the IP shocks with relatively low $M_{ms}$ can perturb large regions ahead of them. Inspection of the spectra further upstream, up to 00:00 UT on August 5, 2009, revealed the existence of magnetic field fluctuations with small relative amplitudes ($\delta B/B \lesssim 0.1$) and featureless spectrum, which do not form part of the ULF wave foreshock.

[28] Figure 4b shows the PLASTIC Wide Angle Partition (WAP) energy spectrum of protons with energies up to 100 keV for the 24-hours interval on August 5, 2009. The spectrum shows enhanced flux of protons with energies ≲1 keV starting ~3 hours upstream of the shock and during 13:00 UT-15:00 UT. There is no enhanced activity of suprathermal (E > 1 keV) ions upstream of the shock.

[29] Figure 5a shows the upstream whistler waves on a 10 second interval adjacent to the shock. The whistlers appear on all four panels. Their amplitudes are largest in the $B_m$ component and smallest in B. They appear to form wave trains with periods of 5 seconds. Their amplitude is largest in the center of the wave trains and smallest between

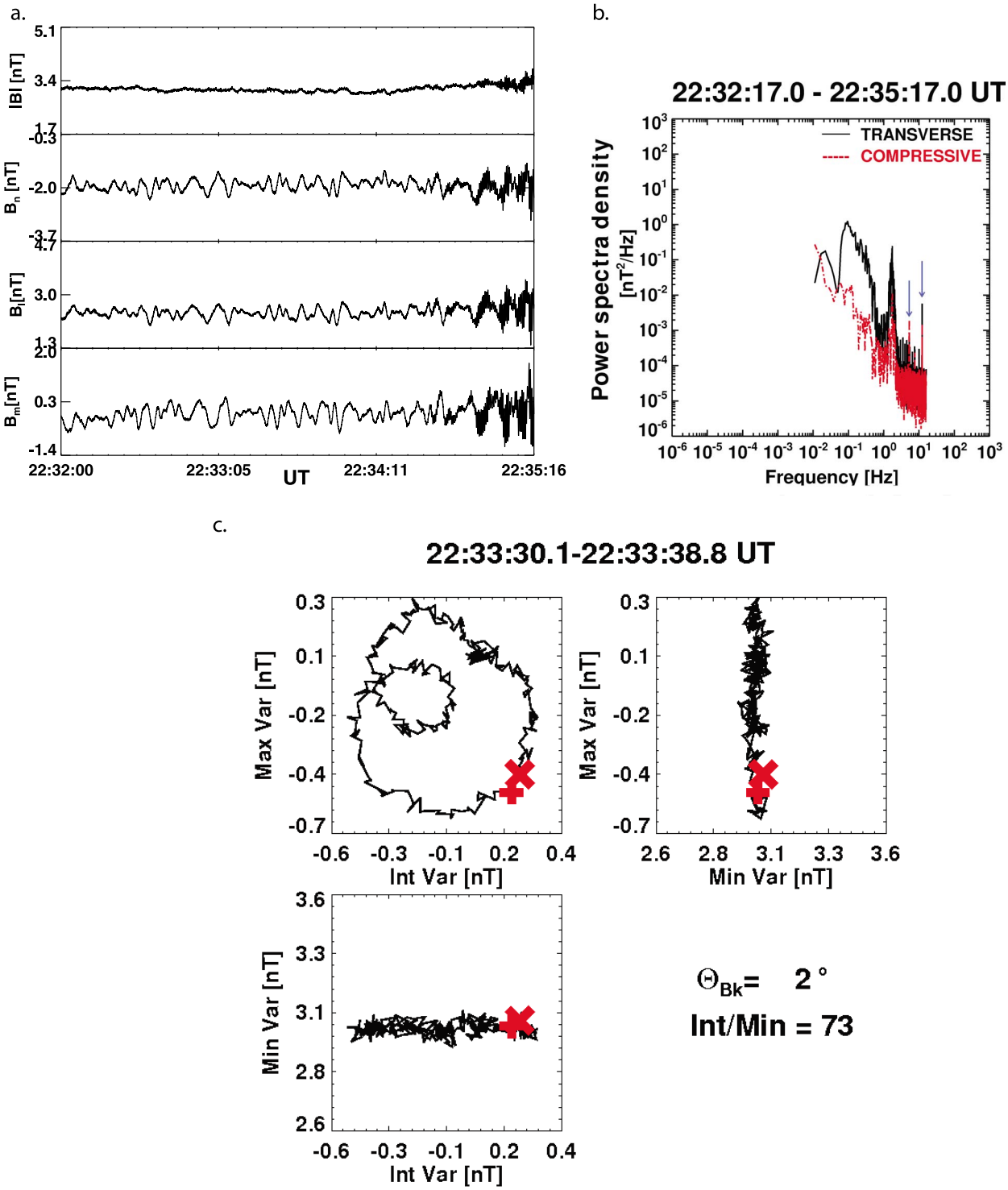


**Figure 3.** (a) Waves upstream of the August 5, 2009 shock. (b) Fourier spectrum of the upstream region. The arrows indicate the strongest peaks caused by the high-frequency, low amplitude noise that is present throughout the 32 Hz data. (c) Hodograms of the upstream waves. The plus and cross signs mark the beginning and the end of the time series.

the trains and on average decreases with the distance from the shock.

[30] The Fourier spectrum in Figure 3b shows that the whistler waves are quite monochromatic with frequencies ~1.8 Hz. They exhibit transverse and compressive components, of which the transverse is stronger. The minimum variance analysis (MVA, Figure 5b) reveals that they are circularly LH polarized in the spacecraft's frame of reference.

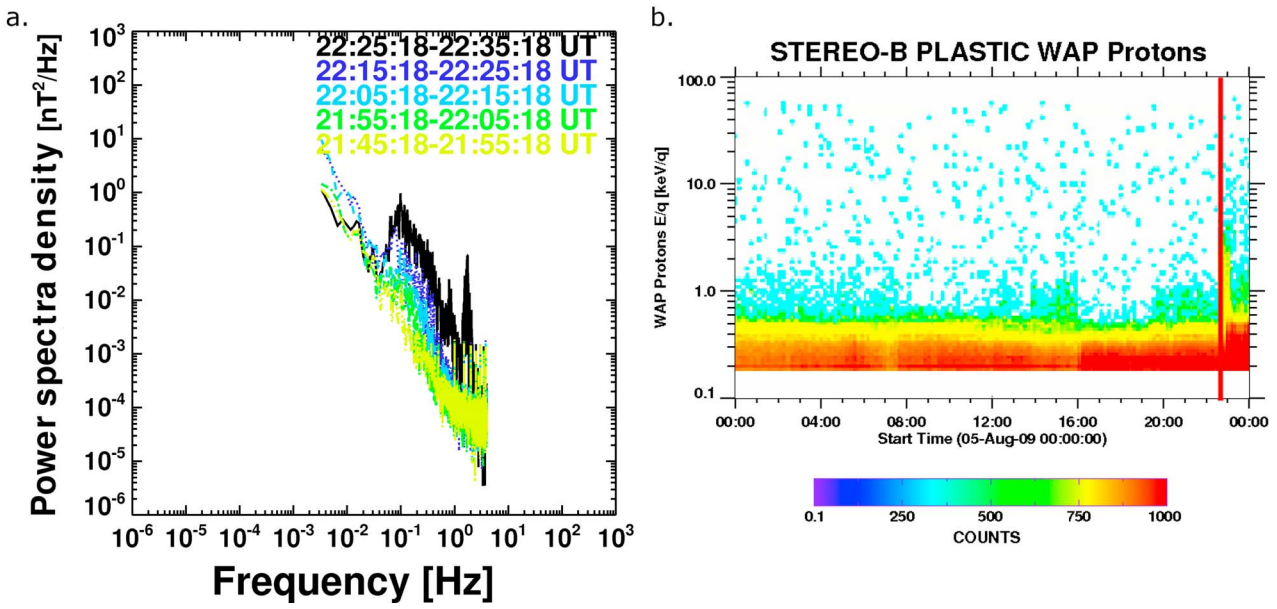


**Figure 4.** (a) Successive Fourier spectra of the transverse component of the ULF waves in the upstream region. (b) PLASTIC WAP energy spectrum of suprathermal protons in the upstream and shock transition regions.

They propagate at $\theta_{Bk} = 9°$ with respect to the upstream IMF and at $\theta_{nk} = 52°$ with respect to the local shock normal. The large $\theta_{nk}$ and the fact that they appear in B and $B_n$ component indicate that these waves are non-standing whistler precursors. The total duration of the whistlers was 42 seconds, which, taking into account the average SW velocity of 377 kms$^{-1}$, corresponds to $\sim 10.6 \times 10^{-5}$ AU.

[31] It is known [see *Russell*, 2007] that whistlers with smaller $\theta_{Bk}$ propagate further upstream from the IP shocks than those that propagate more obliquely to the upstream IMF. Here we analyze properties of upstream whistlers at different distances from the shock and at different locations within the wave trains. We measure the properties of the waves (propagation angles, compressibility, polarization) during small time intervals, several seconds long. These intervals were chosen carefully so that only whistler properties were measured and there was no interference from the larger period (ULF) fluctuations.

[32] In the case of the August 5, 2009 shock we first measure the properties of the whistlers during 22:34:52-22:34:54 UT (upstream of the shock) and 22:35:16.5-22:35:18.5 UT (adjacent to the shock). The measured quantities were the following: $\theta_{Bk}$ = 7° and 33°, $\theta_{nk}$ = 54° and 37°, the ratio Int/Min = 62 and 7 and the polarization was

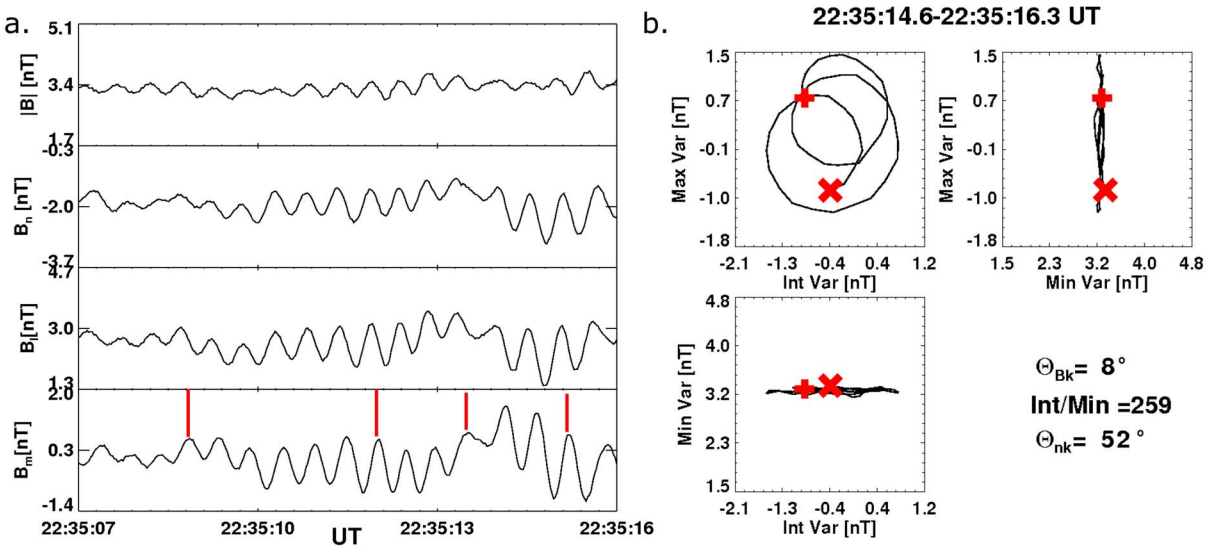


**Figure 5.** (a) Whistler waves upstream of the August 5, 2009 shock. The lines mark the wave fronts studied in the section 2.1.1. (b) Hodogram of the whistler waves. The plus and cross signs mark the beginning and the end of the time series.

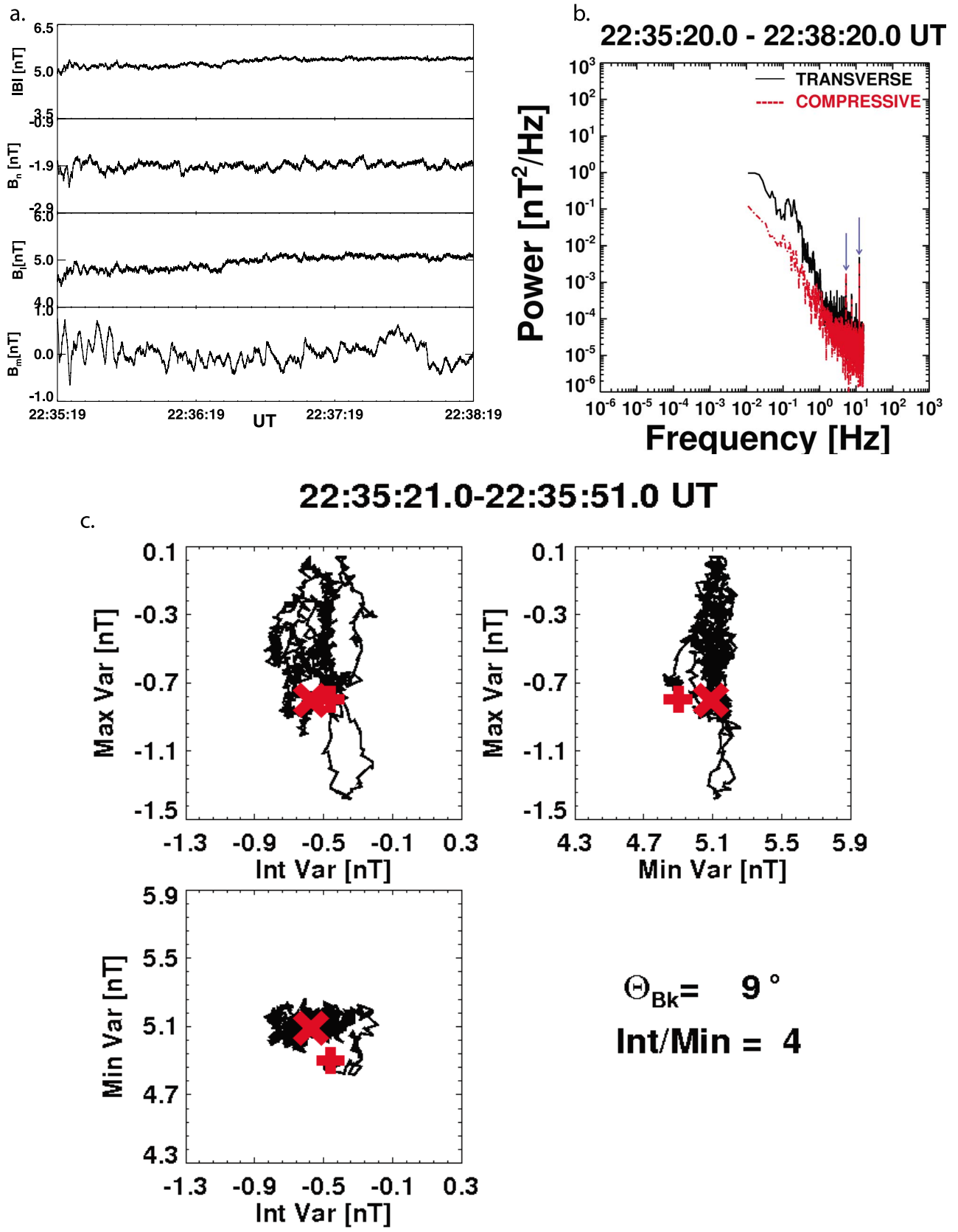


**Figure 6.** (a) Waves downstream of the August 5, 2009 shock. (b) Fourier spectrum of the downstream region. As in Figure 3b, the blue arrows indicate the strongest peaks caused by the high-frequency, low amplitude noise in 32 Hz data. (c) Hodogram of the downstream region.

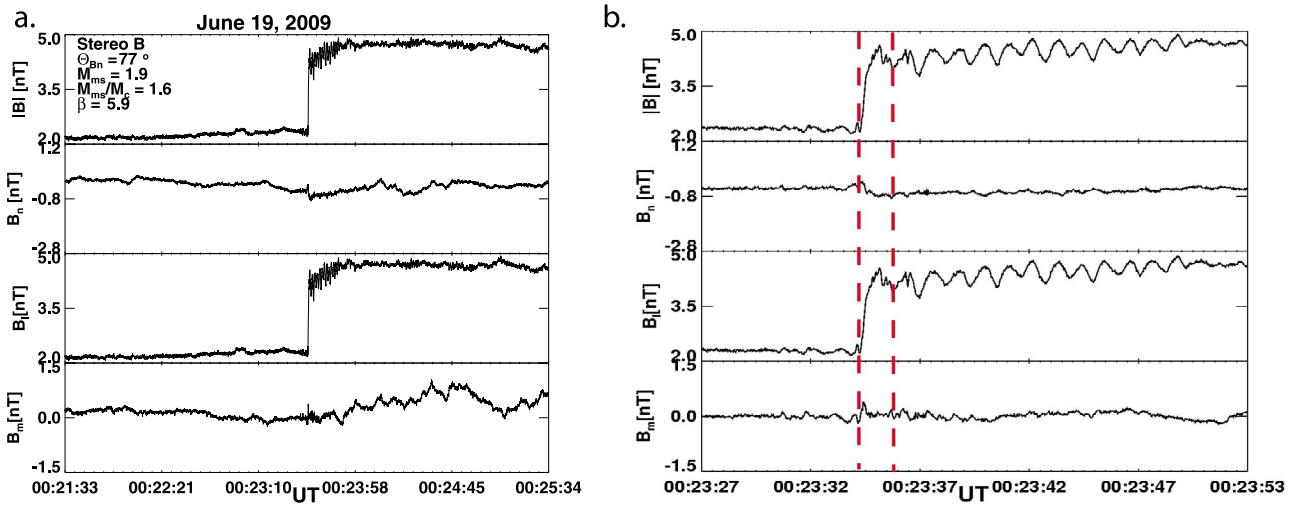


**Figure 7.** The IP shock observed on June 19, 2009. Time resolution of the data is 32 Hz. (a) Four minute time interval including the shock and the adjacent regions. (b) Closeup of the shock.

LH in both cases. Their relative peak-to-peak amplitudes were between $\delta B/B \sim 0.1$–0.5. We did not detect any difference in the peak frequency. It can be seen that the $\theta_{Bk}$ is larger and the Int/Min ratio is smaller closer to the shock. The Int/Min ratio on the interval shown in Figure 5b is 259, which suggests that it does not decrease monotonically with the distance from the shock. For this reason we additionally inspect in detail the properties of four individual wave fronts on the interval 22:35:07 UT-22:25:16.2 UT. The analyzed wave fronts are marked with vertical lines in Figure 5a. Two wave fronts are located in the middle of two wave trains and two are located on their edges. In the middle of the wave trains the Int/Min ratios are 337 and 472 and the $\theta_{Bk}$ angles are 17° and 12°. On the edges of the wave trains the ratios Int/Min are 20 and 11 while the propagation angles $\theta_{Bk}$ are 45° and 24°. Hence in the middle of the wave trains, where the whistlers have the largest amplitudes, the waves are also much more planar and propagate more parallel with respect to the B-field than on the edges of the trains. This behavior was found each time the upstream whistlers appeared in trains. We therefore conclude that although the whistler waves are on average more field aligned and more planar at larger distances from the shock their properties vary substantially within individual wave trains.

[33] The downstream waves observed on August 5, 2009 (Figure 6a) show a large transverse power and are much stronger in the $B_m$ component than in the other two components of the field. They have periods between 10 and 20 seconds (Figure 6b). The corresponding hodograms (Figure 6c) show that they are irregularly polarized and that they propagate at $\theta_{kB} \sim 9°$ with respect to the downstream B-field. It has to be stressed out that the direction of propagation is very uncertain due to the compressive nature of these waves. Their duration in the data is ∼10 minutes, which corresponds to $1.5 \times 10^{-3}$ AU.

[34] It should be mentioned that when examining the waves in the region adjacent to the shocks with 32 Hz resolution data, we found high-frequency (2 Hz–7 Hz), low amplitude ($\delta B/B \sim 0.01$) noise that is present throughout the data. This noise manifests itself in various ways—in the magnetic field panels and hodograms as small, rapid fluctuations superposed onto the real data and in the high-frequency parts of the Fourier spectra as very narrow peaks. These peaks exhibit significant power only in those spectra that were made for time intervals ranging from ∼30 seconds to a few minutes (see Figures 3b, 6b, 9b and 12b ). In these figures the strongest peaks that are due to the noise are marked with blue arrows. On short time intervals of ≤10 seconds for downstream HF waves and upstream whistlers these peaks are very small (see Figure 11b). In most cases the noise does not interfere with the studied waves since it exhibits only very narrow peaks with frequencies that are higher than those of the waves. Only in one case (Figure 14c) do the frequencies of the whistler waves coincide with the frequency range of the noise. However, no noise is observed during this interval.

[35] This noise is different for the data from each spacecraft, but it always appears at roughly the same frequencies in the data provided by the same spacecraft.

### 2.1.2. June 19, 2009 Event

[36] Figure 7 presents an IP shock observed on June 19, 2009 at 00:23:34 UT by STEREO B which is driven by a MC observed from June 19, 2009 07:40 UT to June 20, 2009 10:00 UT. 32 Hz resolution is used for the magnetic field data. The upstream SW speed was 300 $kms^{-1}$. This is a quasi-perpendicular shock ($\theta_{Bn} = 77°$) with $M_{ms} = 1.9$, ratio of criticality ($M_{ms}/M_c$) 1.6 and the upstream beta is 5.9.

[37] Figure 7a shows B-field components and magnitude during the four minutes, when the shock was observed. The shock itself and the immediate upstream and downstream regions can be appreciated. The shock exhibits a well defined ramp across which the B-field magnitude increases rapidly. The ramp is followed by HF fluctuations that extend ∼15 s downstream of the shock. The average upstream value of B is ∼2.3 nT, while in the downstream region it settles at 4.2 nT, so their ratio is 1.9.

[38] Figure 7b shows the detailed structure of the shock in 32 Hz resolution. The duration of the ramp delimited by two vertical lines is ∼1 second. In contrast to the previous case

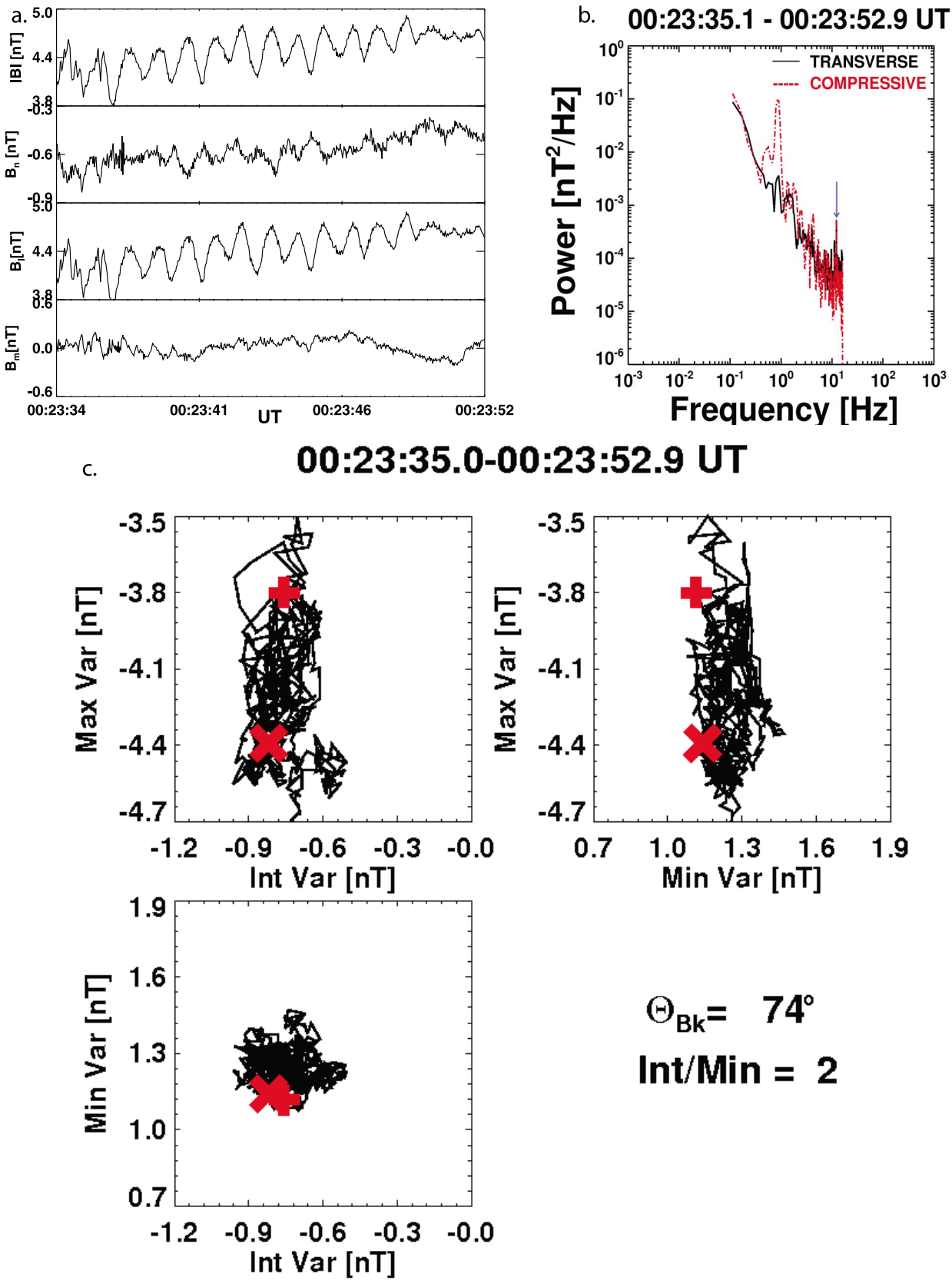


**Figure 8.** (a) Waves downstream of the June 19, 2009 shock. (b) Fourier spectrum of the downstream region. The blue arrow indicates the strongest peak caused by noise in the 32 Hz data. (c) Hodogram of the downstream region.

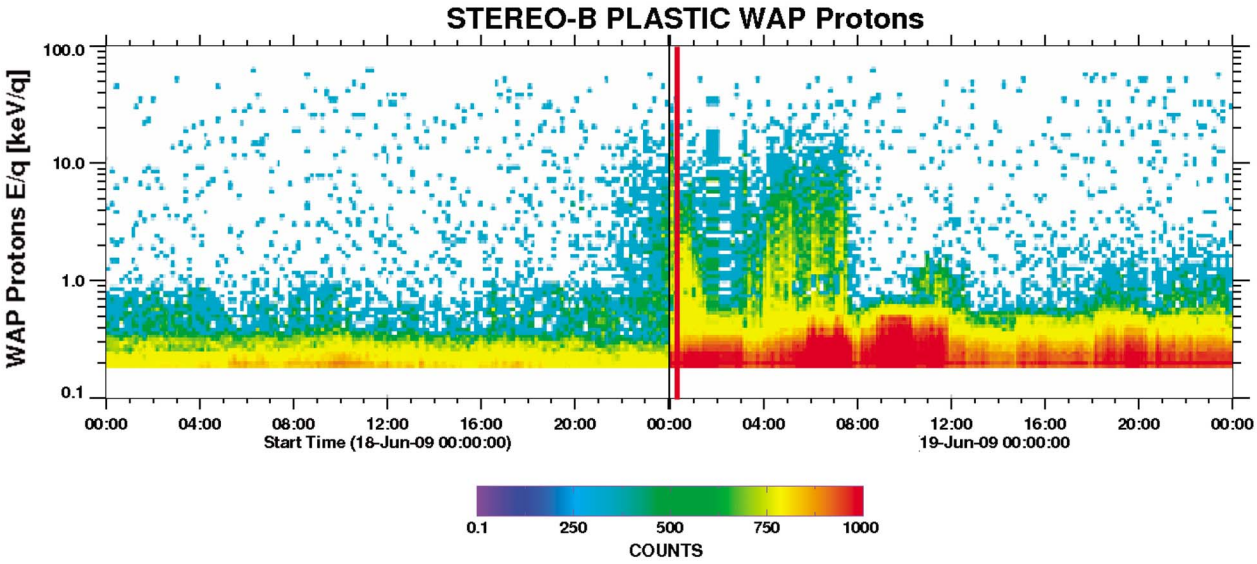


**Figure 9.** PLASTIC WAP energy spectrograms of suprathermal protons during June 18, 2009 and June 19, 2009.

study, this quasi-perpendicular shock does not have an overshoot and no waves are found upstream.

[39] In Figure 8a we present the downstream fluctuations. In the top panel with the magnitude of the field, there are 13 wave fronts during the first 15 seconds, which means that their periods are 1.15 seconds. This corresponds to a frequency of 0.87 Hz. The following panels reveal that these waves exhibit the largest amplitudes in the $B_l$ component. Also present are the variations of the $B_m$ component but with much smaller amplitudes and a phase difference $\pi/2$. These are strongly damped and appear only in the interval $\sim$5 seconds downstream of the shock. This means that downstream fluctuations begin as very elliptically, almost linearly polarized waves and eventually become completely linearly polarized. The fluctuations of the $B_n$ component have amplitudes $\Delta B_m < \Delta B_n < \Delta B_l$. Their phase differs from that of the B fluctuations by $\pi$.

[40] Figures 8b and 8c show the power spectrum and the MVA of the HF downstream waves, respectively. In the Fourier spectrum these waves peak at frequencies $\sim$0.9 Hz. They exhibit a strong compressive component, while their transverse component is much weaker. In accordance, the MVA reveals that the 0.9 Hz waves are compressive and linearly polarized. The ratio Int/Min is 2.0, due to which their calculated angle of propagation is very uncertain, being $\theta_{Bk} = 82^\circ \pm 55^\circ$. We used the method described in *Hoppe et al.* [1981] in order to estimate this uncertainty.

[41] The PLASTIC WAP data (Figure 9) show that an enhanced suprathermal proton flux ($E \lesssim 10$ keV) was observed during $\sim$1.5 hours before the shock arrival. Also,

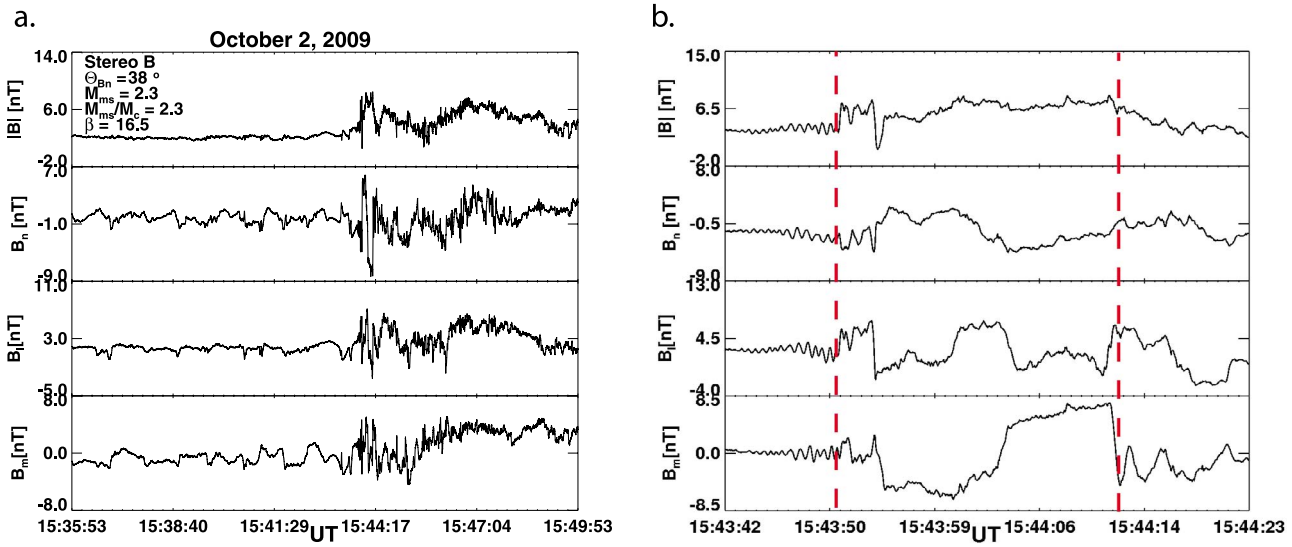


**Figure 10.** The shock observed on October 2, 2009. Time resolution of the B-field data is 32 Hz. (a) Fourteen minute time interval including the shock and the adjacent regions. (b) Closeup of the shock.

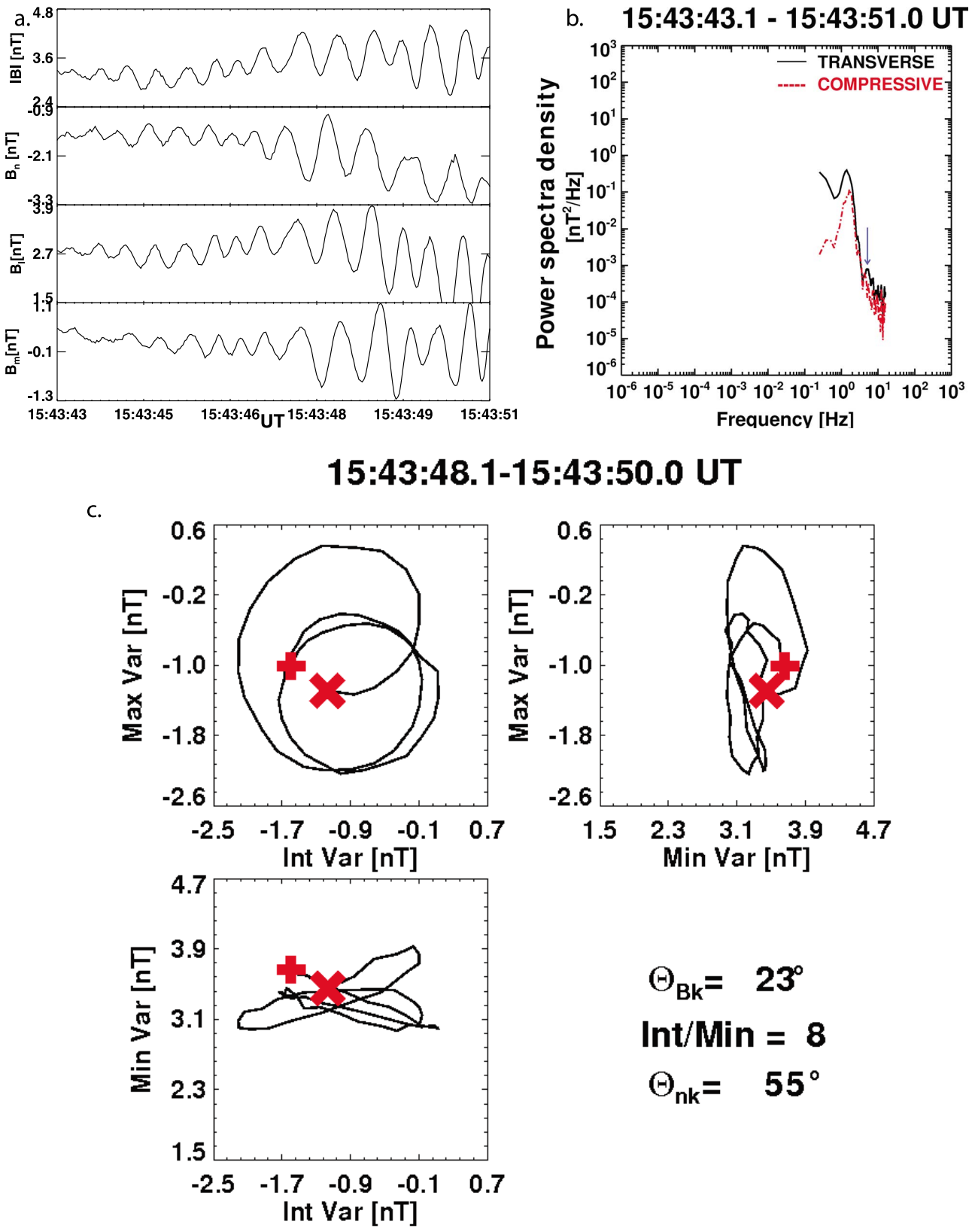


**Figure 11.** (a) Whistler waves upstream of the October 2, 2009 shock. (b) Fourier spectrum of the upstream whistler waves. The vertical blue arrow indicates the noise in the 32 Hz data. (c) Hodogram of the whistler waves.

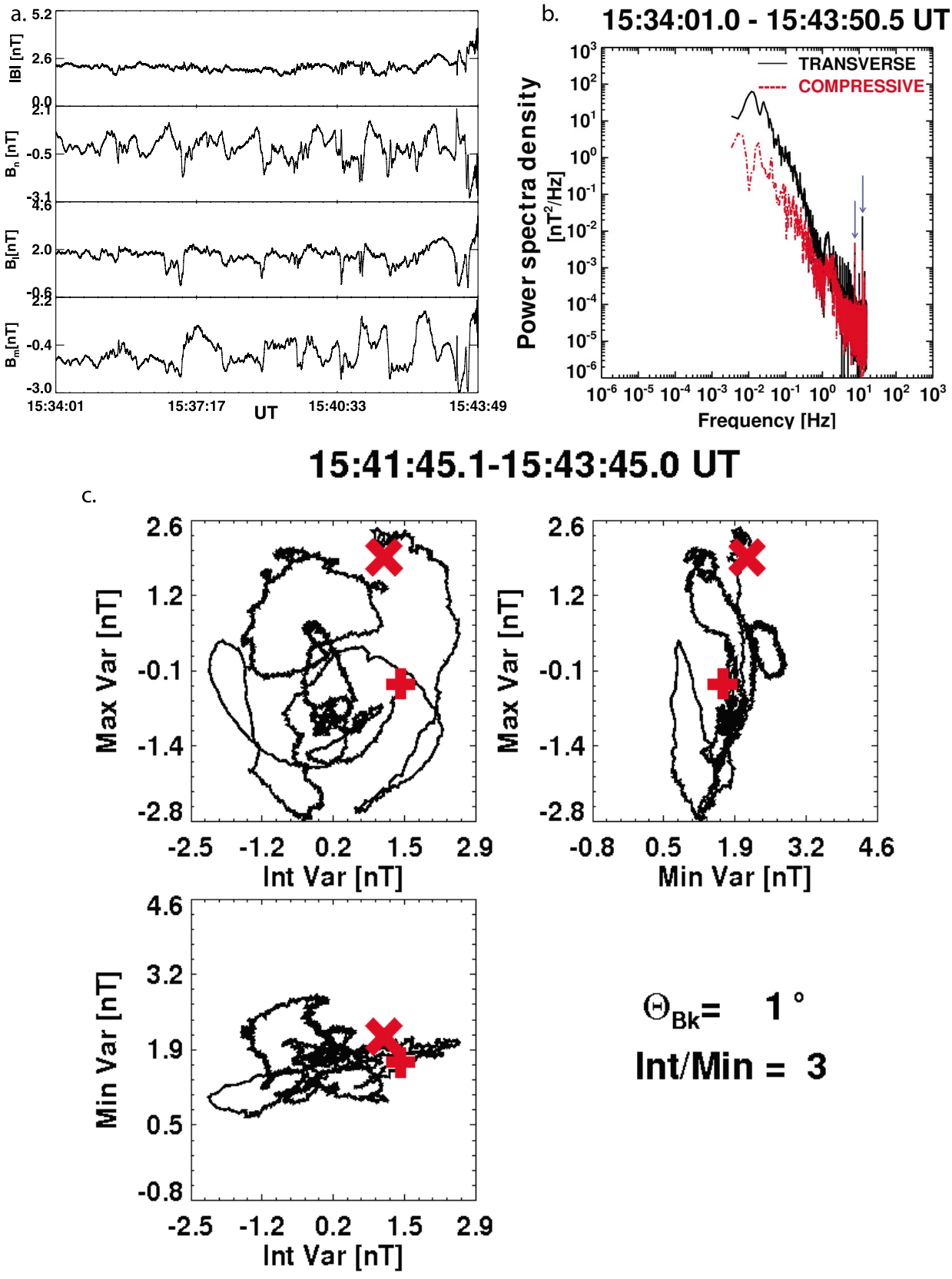


**Figure 12.** (a) Waves in the upstream region of the October 2, 2009 shock. (b) Fourier spectrum of the upstream region. The arrows indicate the peaks caused by noise in the 32 Hz data. (c) Hodogram of the upstream waves.

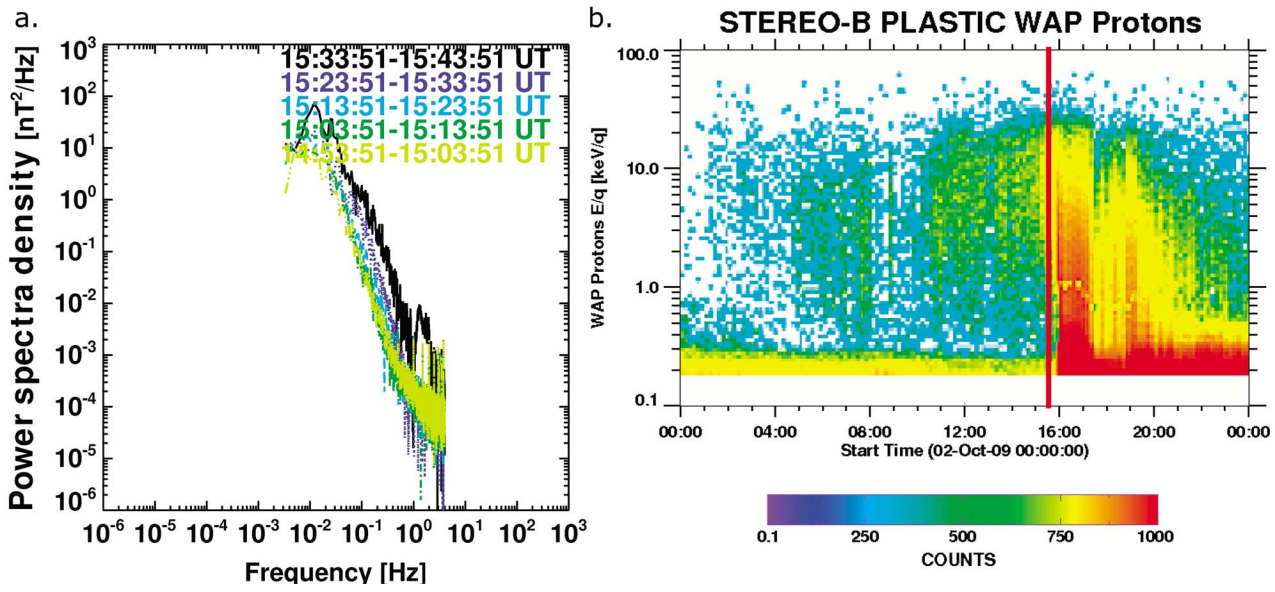


**Figure 13.** (a) Spectra of the transverse component of the ULF waves in the foreshock region of the October 2, 2009 shock. (b) Energy spectrum of suprathermal protons in the upstream region observed by the PLASTIC WAP instrument.

proton fluxes with similar energies appear in the downstream region.

### 2.1.3. October 2, 2009 Event

[42] The third case study presented here was observed on October 2, 2009 with a shock observed at 15:43:50 UT by the STEREO B spacecraft (Figure 10a). After 15 hours the shock was followed by an ICME. This is the only quasi-parallel ($\theta_{Bn}$ = 38°)shock in our sample. Due to the quasi-parallel geometry, the shock transition is not as sharp as in the previous two cases (Figure 10b). The shock's $M_{ms}$ is 2.3, its criticality ratio is 2.3 and the upstream beta is 16.5, which is by far the highest value in the sample. Figure 10b shows a closeup of the shock and its immediate upstream and downstream regions. It can be seen that the shock transition region is very different from the previous two. It is very irregular and with a larger extension. It exhibits strong variations of the B-field magnitude and field rotations can be appreciated during the transition. These last from ~15:43:53 UT until 15:44:13 UT, i.e., 20 s in total. Magnetic field data in both figures have a time resolution of 32 Hz.

[43] The region immediately upstream of the shock is populated by whistler waves (Figure 11a) that extended 8 s ($1.8 \times 10^{-5}$ AU) upstream of the shock. They appear in two wave trains. Their amplitudes diminish with increasing distance from the shock. Their Fourier spectrum (Figure 11b) shows that the waves exhibit transverse and compressive components, with the first being stronger. Their power peaks at f ~ 1.3 Hz. The hodograms in Figure 11c also show that the whistlers appear with different amplitudes. They propagate at angles $\theta_{Bk}$ = 23° and $\theta_{kn}$ = 55° and their Int/Min ratio is 8.

[44] We additionally analyze the whistlers during two short time intervals at 15:43:47–15:43:48.5 UT and 15:43:50-15:43:51.5 UT (not shown). Even though the total time interval during which the whistlers were present was very short, their properties changed. The $\theta_{Bk}$ changed from 38° to 49° and the Int/Min ratio diminished from 13 to 9 closer to the shock. The corresponding $\theta_{nk}$ values were 76° and 22°. Their relative peak-to-peak amplitudes ranged from ~0.1 to ~0.7. As in the first case study, the upstream whistlers on average exhibited smaller amplitudes, were more field aligned and more planar when located further upstream of the shock, but further inspection of individual wave fronts showed that these properties vary within the wave trains and are not monotonic functions of the distance from the shock.

[45] The properties of upstream ULF fluctuations observed from 15:34:00 UT to 15:43:50 UT are presented in detail in Figures 12a, 12b and 12c. It can be seen that the amplitudes of these waves are larger in B-field components than in B. Hence these waves are mostly transverse. Their spectrum is mostly featureless and the transverse component dominates during the entire time interval presented. The hodograms show that these waves consist of many irregular fluctuations with different amplitudes and frequencies.

[46] In Figure 13a we can see that upstream ULF waves are observed only during the first twenty minutes upstream of the shock. This corresponds to a distance of $\sim 2.2 \times 10^{-3}$ AU.

[47] Visual inspection of magnetic field time series shows that B-field fluctuations exist upstream of this shock for a region which is larger than the ULF waves region, where spectra show clear peaks. These fluctuations have amplitudes $0.1 \lesssim \delta B/B \lesssim 0.3$ and are observed up to 70 minutes from the shock transition, i.e., $8.0 \times 10^{-3}$ AU. Because these fluctuations exhibit a broad featureless spectra with frequencies in the range $10^{-3}$–10 Hz we do not consider them to be part of the ULF foreshock. They can however participate in the acceleration of particles to suprathermal energies and contribute to SW modification ahead of the shock.

[48] The PLASTIC WAP data (Figure 13b) reveal the presence of enhanced fluxes of suprathermal protons ~9 hours before the observation of the shock. By multiplying this time with the upstream SW speed (300 $kms^{-1}$) we obtain a

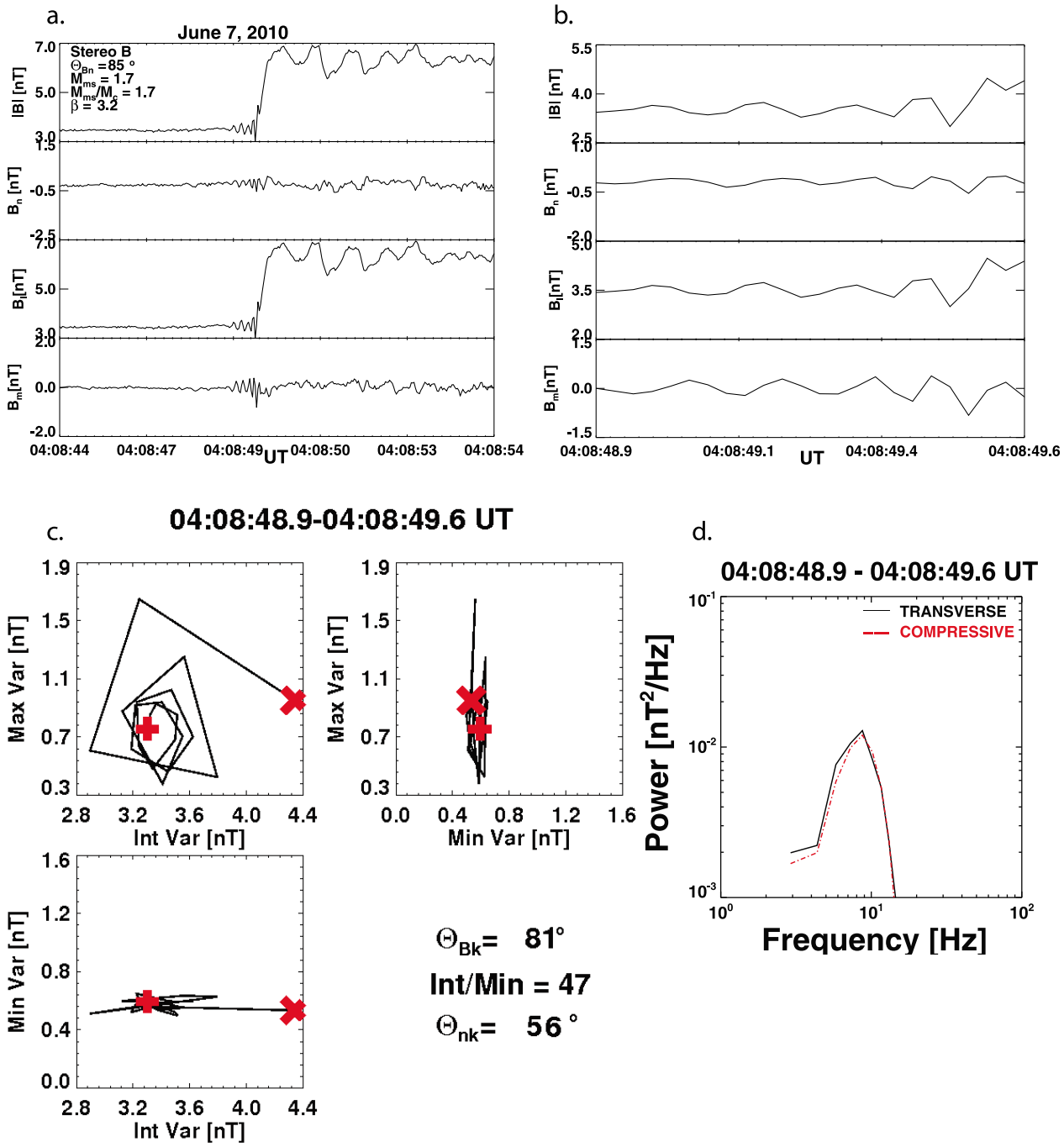


**Figure 14.** (a) June 7, 2010 shock and its adjacent regions. (b) Waves in the upstream region. (c) Hodogram of the upstream waves. (d) Fourier spectrum of the waves.

proxy of the suprathermal proton foreshock extension $\sim 6.5 \times 10^{-2}$ AU.

## 3. Summary of Shock and Waves Properties

[49] We examined 10 IP shocks formed due to the interactions between ICMEs and the solar wind. In seven cases 32 Hz B-field data were available. This is the highest time resolution at which the magnetic field profiles of the IP shocks have been observed. This allows us to study the shocks and associated waves in more detail than ever before.

[50] Nine ICMEs (90%) were magnetic clouds (MCs). Such high proportion of MCs is not surprising. In their studies *Richardson and Cane* [2004] and *Jian et al.* [2011] concluded that the fraction of ICMEs that are MCs during solar minimum reaches ∼100%.

[51] The average and the median ICME velocities in our sample are 440 $kms^{-1}$ and 405 $kms^{-1}$, respectively. In a

study of ICME driven shocks and their drivers observed during the Solar cycle 23, *Gopalswamy et al.* [2010] found the average and the median ICME velocities to be 527 $kms^{-1}$ and 470 $kms^{-1}$, which is more than our values. Only two (20%) ICMEs from our sample had velocities above 527 $kms^{-1}$. This is in agreement with *Jian et al.* [2011], who reported lower average ICME speeds during solar minimum.

[52] The shocks in our sample exhibit a wide range of parameters. Nine (90%) are quasi-perpendicular ($\theta_{Bn} \geq 45°$). Seven events (70%) exhibit $\theta_{nR} \leq 45°$. Nine (90%) have $M_{ms} \leq 2$. The average $M_{ms}$ in the sample is 1.7. Nine shocks (90%) are supercritical ($M_{ms}/M_c > 1$), and the upstream betas range from 0.9 to 16.5.

### 3.1. ULF Waves and Suprathermal Particles

[53] Coherent waves appear upstream and/or downstream of all supercritical shocks, while no coherent waves were observed in the regions adjacent to the subcritical shock.

[54] The ULF waves (~10 s–30 s) appear upstream of three shocks (30%) and downstream of three (30%) events. It was considered that the ULF waves exhibit enhanced activity if a bump appears in the power spectra of the B-field data in the shock's upstream/downstream regions. Typical amplitudes of ULF waves were found to be $\delta B/B > 0.3$, but they can be as large as $\gtrsim 1$ just next to the shock transition. The upstream ULF waves show no evidence of steepening. In the past shocklets have been observed upstream of IP shocks with Mach number ~4 [*Wilson et al.*, 2009]. The lack of these structures upstream of the shocks in our sample could be due to their small $M_{ms}$. For the three cases with enhanced upstream ULF wave activity we perform an additional analysis to determine the foreshock's extensions as observed by the spacecraft. We calculated the Fourier power spectra for consecutive upstream 10-minute time intervals and inspected them for the presence of ULF waves.

[55] In the spacecraft's frame of reference the ULF wave foreshock extended $4.6 \times 10^{-3}$ AU upstream of the quasi-perpendicular August 5, 2009 shock (largest foreshock in the sample), $2.2 \times 10^{-3}$ AU upstream of the quasi-parallel October 2, 2009 shock, and $2.5 \times 10^{-3}$ AU upstream of the quasi-perpendicular April 23, 2010 shock. However, mostly transverse magnetic field fluctuations with featureless spectra in the ULF wave frequency range and with amplitudes $0.1 \lesssim B/B \lesssim 0.3$, can extend even further upstream. Such fluctuations may also contribute to the acceleration of ions to suprathermal energies. We find these fluctuations upstream of October 2, 2009 and January 25, 2009 shocks, extending ~$8.0 \times 10^{-3}$ AU and ~$9.2 \times 10^{-3}$ AU, respectively.

[56] The fact that the regions upstream of quasi-perpendicular August 5, 2009 and April 23, 2010 shocks were permeated with ULF waves is unexpected and in contrast to the regions upstream of the quasi-perpendicular Earth's bow-shock which are quiet, without ULF fluctuations. There are three possible explanations for this:

[57] 1. It could be that the shocks were quasi-parallel prior to the spacecraft's observations and that the foreshocks also formed prior to that.

[58] 2. The geometry of the IP shocks is different for different points on the shock front [*Greenstadt and Mellott*, 1985; *Jian et al.*, 2009a; *Aguilar-Rodriguez et al.*, 2011]. It could be that adjacent to the observed IP shocks there were quasi-parallel shocks. Upstream of these adjacent shocks the ULF waves would be excited by backstreaming ions, thereby forming foreshock regions. A portion of these waves may have propagated in such a way that they populated the regions upstream of the observed quasi-perpendicular shocks. Also, depending on the spacecraft's orbit relative to shock surface, part of the ULF wave foreshocks observed by the spacecraft might have been located upstream of these adjacent shocks and not upstream of the shocks that was later observed.

[59] 3. In the case of the August 5, 2009 event we note that the properties of the upstream waves are very similar to those of the ion cyclotron waves (ICWs) described by *Jian et al.* [2009b]. These waves are likely formed near the solar corona, they propagate almost parallel to the IMF and exhibit frequencies below the local proton gyrofrequency in the solar wind frame. They are intrinsically circularly LH polarized, transverse and show narrow spectra. They tend to appear when the radial component of the IMF is strong, so that the IMF and the direction of SW speed are almost parallel ($\theta_{Br} \lesssim 30°$). In the case of the August 5, 2009 shock the average upstream $\theta_{Br}$ was ~33°. If the observed waves are indeed the ICW waves then they were not produced by the shock and it is only a coincidence that they appear in its upstream region.

[60] Numerical studies show that the $\theta_{Bn}$ angle of IP shocks changes with time on different temporal and spatial scales. MHD simulations performed by *Rouillard et al.* [2011] suggest that during the shock's propagation its upstream configuration changes gradually along the whole shock front. Another possible mechanism is described by *Krauss-Varban et al.* [2008], who performed hybrid simulations of oblique, planar shocks, similar to those in IP space. These authors found that upstream compressional waves which are carried towards the shocks continuously bend the upstream IMF lines and thus locally change the $\theta_{Bn}$. Some portions of the shocks become more parallel and others more perpendicular. The former can eject more protons in the upstream direction and further enhance the amplitudes of the upstream compressional waves. The more parallel sections travel together with the shock surface which leads to its "undulation". One would expect that this mechanism acts on spatial and temporal scales that are similar to the wavelengths and periods of the upstream compressive waves and are therefore much smaller than the scales described by *Rouillard et al.* [2011]. We can even imagine the local $\theta_{Bn}$ oscillating around some average value with the latter depending on the location on the shock front and changing gradually with time. The suprathermal ions could then appear upstream of what in principle are quasi-perpendicular sections of the IP shocks but they would be more intense upstream of their quasi-parallel sections.

[61] We also inspected the PLASTIC WAP data for the presence of suprathermal ($1 \text{ keV} \leq E \leq 20 \text{ keV}$) protons upstream of the shocks to know if they are preceded by ion foreshocks. In the case of the terrestrial bow shock, the backstreaming suprathermal ions interact with the incoming solar wind plasma and can generate ULF waves. The regions of the ULF wave and the suprathermal ion foreshocks spatially almost coincide.

[62] If the same was true for the IP shocks then we would expect to observe the suprathermal particles whenever

upstream ULF waves appear. However, enhanced suprathermal proton flux was detected upstream of five IP shocks (50%, Table 2), four of which were quasi-perpendicular with no ULF wave foreshock. No suprathermal particles were observed upstream of the quasi-perpendicular, August 5, 2009 shock, that exhibited the most extended ULF wave foreshock. The shocks observed on June 7, 2010 and April 23, 2010 exhibited the largest suprathermal proton foreshocks (0.19 AU and 0.23 AU, respectively), although the first shock had no ULF wave foreshock and the extent of the ULF wave foreshock associated with the second shock was $\sim$100 times smaller than that of the suprathermal proton foreshock. The enhanced suprathermal proton fluxes associated with the April 23, 2010 shock were observed as early as 11 hours before the shock. In the case of the quasi-parallel October 2, 2009 shock (Figure 13b), the enhanced upstream suprathermal proton flux begins $\sim$9 hours before the observation of the shock.

[63] We should note that calculating the extents of foreshocks gives us only a rough proxy of their true extensions since we have no way of knowing how the spacecraft crossed them.

[64] The four shocks with suprathermal proton foreshocks but no enhanced upstream ULF waves exhibit $\theta_{Bn} \geq 68°$. The protons could have been energized at the shocks themselves and then reflected back upstream if the shock's geometry permitted it at some point in the past. Alternatively, they could have leaked from the shock sheath regions. The absence of waves suggests that backstreaming ion distributions did not fulfill the conditions necessary to overcome instability threshold. A detailed analysis of the ion distribution functions (density, velocity, temperature, anisotropy) is needed to determine if ion-ion instabilities, such as the right-hand and LH resonant modes [*Gary et al.*, 1984, 1985; *Gary*, 1985] can grow in these regions.

[65] The October 2, 2009 shock is the only quasi-parallel in the sample. It exhibits the highest upstream plasma $\beta$ (16.5). An extended suprathermal proton foreshock was observed several hours before the shock. It is known from the studies of planetary bow-shocks that stronger (higher $M_{ms}$, and larger $M_{ms}/M_c$), quasi-parallel shocks can reflect more suprathermal particles into the upstream region. These particles interact with the upstream IMF, exciting the ULF waves [*Gary*, 1993]. Ion distribution functions become wider due to wave-particle interactions and therefore their temperature rises, which results in higher upstream $\beta$.

### 3.2. Upstream HF Waves

[66] Another type of waves that was observed upstream of the shocks were the whistler precursors. The whistlers were observed upstream of seven shocks (70%). We call the upstream region permeated by these waves the HF wave foreshock. The sizes of these regions range from $2 \times 10^{-6}$–$2 \times 10^{-4}$ AU (Table 2).

[67] The upstream whistlers commonly appear in wave trains. Their properties change with the distance from the shock and within individual trains. The wave fronts further upstream of the shocks are on average less compressive (larger Int/Min ratio) and are propagating more parallel to the upstream IMF (smaller $\theta_{Bk}$) than those closer to the shocks. Also, their amplitudes diminish on average with the distance from the shocks. Within individual wave trains the whistler amplitudes are largest in the middle of the trains and smallest in their edges. The wave fronts in the middle are more planar and tend to propagate more parallel with respect to the upstream IMF direction.

[68] The whistlers in our sample propagated at $\theta_{Bk}$ between 10° and 80° and at $\theta_{nk}$ between 20° and 90°. In one case (August 5, 2008) the waves further upstream of the shock propagated at $\theta_{Bk} = 6°$, but closer to it this angle was 33°. These whistlers are not phase standing, since this would require very small $\theta_{kn}$, but rather they are similar to those described by *Russell* [2007], *Wilson et al.* [2009] and others. This is probably because the phase standing whistler precursors appear upstream of laminar quasi-perpendicular shocks with upstream $\beta \ll 1$ [e.g., *Mellott and Greenstadt*, 1984; *Duboulz and Scholer*, 1993]. The upstream $\beta$ in our sample range from 0.9 and 16.5, so the shocks are not laminar.

[69] Whistlers with even higher frequencies were observed upstream of the June 7, 2010 event. This is the most quasi-perpendicular case ($\theta_{Bn} = 85°$). The waves could be analyzed due to the high time resolution (32 Hz) of the B-field data. Just upstream of the shock's ramp, between 04:08:48.8 UT and 04:08:49.6 UT (0.8 seconds), there is a wave train with several wave fronts. Figure 14 shows the shock and the waves in the shock-normal coordinate system, the closeup of the waves and the corresponding hodograms. The FFT analysis shows (Figure 14d) that the peak frequency of the waves is 8.8 Hz. They propagate at angles $\theta_{Bk} = 81°$ and $\theta_{nk} = 56°$ and their Int/Min ratio is 47. They appear as LH polarized fluctuations. It is interesting that these waves propagate at such a large angle and that they are so transverse and circularly polarized (Max/Int is $\sim$1).

[70] The observed properties of upstream ULF and whistler waves can be explained in terms of their formation mechanism and the degree of damping that they suffer. The ULF waves have group velocities that are smaller than the velocities of IP shocks (these are similar to the Alfven speed which at 1 AU is $\sim$50 $kms^{-1}$). They must therefore be formed locally by beam instabilities. In the case of planetary shocks, the ULF waves have simple forms further upstream and they steepen and become more compressive as they are convected towards the shock fronts. In the case of the ULF waves in our sample no steepening has been observed. It is possible that particle density gradients are not strong enough to cause the steepening [*Scholer*, 1993]. Alternatively the IP shocks could catch up with the waves before they can steepen substantially.

[71] The HF upstream waves belong to the whistler branch. Their group velocities exceed those of the IP shocks so these waves may propagate away from them. The whistler waves are Landau damped, so that their amplitude on average diminishes with the distance from shock fronts. Waves that propagate more parallel to the upstream IMF experience less Landau damping than more obliquely propagating waves. Therefore further away from the shocks the HF waves tend to be more field aligned and less compressive.

### 3.3. Downstream HF Waves

[72] We observe coherent HF fluctuations with frequencies $\sim$0.9 Hz downstream of four (40%) IP shocks (Figure 7). Similar fluctuations were first discovered by *Balikhin et al.* [2008] in the bow shock of Venus. Their amplitudes are

largest in the $B_l$ component of the B-field, while in the $B_m$ component they are much smaller. Their relative phases differ by $\pi/2$. The fluctuations of the $B_m$ component are heavily damped and tend to disappear after $\sim$5 s. The polarization of these waves changes from very elliptical, almost linear to completely linear. The $B_n$ component also fluctuates with amplitudes that are between those of $B_l$ and $B_m$ and exhibit a phase difference of $\pi$ relative to the B fluctuations.

## 4. Conclusions

[73] We performed a study of waves around ten ICME associated IP low Mach-number shocks observed by STEREO spacecraft during the years 2007–2010. This is the first attempt to systematically study micro-scale structures in regions around IP shocks driven by ICMEs. The shocks were observed during a minimum of solar activity, when most ICMEs had moderate velocities. The ICMEs were isolated phenomena, meaning that the spacecraft observed one ICME at the time instead of the superposition of various ICMEs or ICMEs and SIRs (which can be observed during the maximum of solar activity). Here we briefly summarize the most important results of this work:

[74] 1. No phase standing whistler precursors were observed upstream of shocks in our sample even though the $M_{ms}$ of the shocks were low ($\leq$2.3). This is due to the fact that none of the shocks was laminar since their upstream betas were not $\ll$1 [e.g., *Duboulz and Scholer*, 1993].

[75] 2. It is the first time we observe fluctuations, similar to those reported by *Balikhin et al.* [2008] in the foreshock of Venus, downstream of ICME driven IP shocks. *Russell et al.* [2009] reported such fluctuation downstream of IP shocks, but did not discriminate between SIR driven and ICME driven shocks. The majority of the shocks in their sample were probably SIR driven.

[76] 3. In the case of upstream whistlers that are modulated in wave trains, the properties of wave fronts depend on their location in the train. The wave fronts in the middle of the trains have larger amplitudes, are more planar and propagate more parallel to the B-field direction. The average whistler properties also change with the distance from the shock. Closer to the shock transition the wave fronts are more compressive on average and propagate more obliquely with respect to the upstream IMF.

[77] 4. We show that even IP shocks with small $M_{ms}$, such as those in our sample, can perturb large regions in front of them.

[78] 5. We exhibit several shocks with quasi-perpendicular geometry and with ULF/proton foreshocks in their upstream region. In some cases only ULF wave or suprathermal proton foreshock exists. When both are present, they can have very different extensions in the data.

[79] 6. The shock fronts that precede ICMEs can be very complex. Their forms vary in space and they change with time [e.g., *Rouillard et al.*, 2011; *Krauss-Varban et al.*, 2008]. The latter is especially important. The IP shocks start perturbing their upstream regions from the moment they are formed. The phenomena observed in these regions, such as waves and suprathermal particles, depend on the history of the shock's geometry. However, the observed geometry of the shocks is an instantaneous property and this may be the reason why we observe ULF waves and suprathermal ions upstream of quasi-perpendicular shocks. In order to study the impact that upstream ULF waves have on the surface of IP shocks, multispacecraft observations with small separation between them will have to be performed in the future. The spacecraft would have to be separated by distances that are less than or similar to the wavelengths and correlation lengths of the waves. If we suppose that typical wavelengths of the ULF waves upstream of IP shocks are similar to those in the Earth's foreshock ($\sim$1 Earth radius) [see *Hoppe et al.*, 1981; *Le and Russell*, 1990; *Le et al.*, 1993; *Archer et al.*, 2005], and their correlation lengths are several times as large [*Archer et al.*, 2005] then these distances will range between several thousand and several tens of thousands of kilometers.

[80] 7. No wave steepening and therefore no shocklets were observed upstream of the shocks. Steepened waves are a common feature upstream of planetary shocks and have also been observed upstream of few IP shocks with higher $M_{ms}$ [*Wilson et al.*, 2009].

[81] Since the solar activity is currently increasing again, we expect many more ICME driven IP shocks to be observed by the STEREO and WIND missions in the following years. This will enable us to perform statistical studies of transient shocks and of their associated waves. As the solar activity rises, so will the speed of many ICMEs. The associated shocks can be stronger, with higher Mach numbers. It will be interesting to examine the waves that are associated with shocks driven by fast ICMEs and study shock properties as well as the extent of the region they perturb ahead of them. Also, the study of electron distribution functions in the regions near the IP shocks will help to clarify their association with the whistler wave precursors.

[82] **Acknowledgments.** X. Blanco-Cano and P. Kajdič acknowledge the CONACyT project grant 81154 and PAPIIT grant IN-110511-3. E. Aguilar-Rodriguez and P. Kajdič thank CONACyT project grant 101625. J. Luhmann acknowledges the NASA support of the STEREO project. The work at UCLA was supported by NASA's STEREO program through grant NAS5-03131 administered by University of California, Berkeley.

[83] Philippa Browning thanks the reviewers for their assistance in evaluating this paper.

## References

Aguilar-Rodriguez, E., X. Blanco-Cano, C. T. Russell, J. G. Luhmann, L. K. Jian, and J. C. Ramírez Vélez (2011), Dual observations of interplanetary shocks associated with stream interaction regions, *J. Geophys. Res.*, *116*, A12109, doi:10.1029/2011JA016559.

Archer, M., T. S. Horbury, E. A. Lucek, C. Mazelle, A. Balogh, and I. Dandouras (2005), Size and shape of ULF waves in the terrestrial foreshock, *J. Geophys. Res.*, *110*, A05208, doi:10.1029/2004JA010791.

Balikhin, M. A., T. L. Zhang, M. Gedalin, N. Y. Ganushkina, and S. A. Pope (2008), Venus Express observes a new type of shock with pure kinematic relaxation, *Geophys. Res. Lett.*, *35*, L01103, doi:10.1029/2007GL032495.

Biskamp, D. (1973), Collisionless shock waves in plasmas, *Nucl. Fusion*, *13*, 719–740.

Blanco-Cano, X. (2010), Bow shocks in the solar wind: Lessons towards understanding interplanetary shocks, *AIP Conf. Proc.*, *1216*, 459–465.

Duboulz, N., and M. Scholer (1993), On the origin of short large-amplitude magnetic structures upstream of quasi-parallel collisionless shocks, *Geophys. Res. Lett.*, *20*(7), 547–550.

Fairfield, D. H. (1969), Bow shock associated waves observed in the far upstream interplanetary medium, *J. Geophys. Res.*, *74*, 3541–3553.

Fairfield, D. H. (1974), Whistler waves observed upstream from collisionless shocks, *J. Geophys. Res.*, *79*, 1368–1378.

Fairfield, D. H., and W. C. Feldman (1975), Standing waves at low Mach number laminar bow shocks, *J. Geophys. Res.*, *80*, 515–522.

Farris, M. H., C. T. Russell, and M. F. Thomsen (1993), Magnetic structure of the low beta, quasi-perpendicular shock, *J. Geophys. Res.*, *98*(A9), 15,285–15,294.

Feldman, W. C., R. C. Anderson, S. J. Bame, S. P. Gary, J. T. Gosling, D. J. McComas, M. F. Thomsen, G. Paschmann, and M. M. Hoppe (1983), Electron velocity distributions near the Earth's bow shock, *J. Geophys. Res.*, *88*, 96–110.

Galvin, A. B., et al. (2008), The Plasma and Suprathermal Ion Composition (PLASTIC) investigation on the STEREO observatories, *Space Sci. Rev.*, *136*, 437–486, doi:10.1007/s11214-007-9296-x.

Gary, P. S. (1985), Electromagnetic ion beam instabilities: Hot beams at interplanetary shocks, *Astrophys. J.*, *288*, 342–352.

Gary, P. S. (1993), *Theory of Space Plasma Microinstabilities*, Cambridge Univ. Press, Cambridge, U. K.

Gary, P. S., C. D. Madland, and B. T. Tsurutani (1984), Electromagnetic ion instabilities: II, *Phys. Fluids*, *27*, 1852–1862.

Gary, P. S., C. W. Smith, M. A. Lee, M. L. Goldstein, and D. W. Fooslund (1985), Electromagnetic ion instabilities, *Phys. Fluids*, *28*, 3691–3695.

Giacalone, J., S. J. Schwartz, and D. Burgess (1993), Observations of suprathermal ions in association with SLAMS, *Geophys. Res. Lett.*, *20*, 149–152.

Greenstadt, E. W., and M. M. Mellott (1985), Variable field-to-normal angles in the shock foreshock boundary observed by ISEE 1 an ISEE 2, *Geophys. Res. Lett.*, *12*, 129–132.

Greenstadt, E. W., R. W. Fredricks, F. L. Scarf, C. T. Russell, R. R. Anderson, and D. A. Gurnett (1981), Whistler mode wave propagation in the solar wind near the bow shock, *J. Geophys. Res.*, *86*, 4511–4516.

Gopalswamy, N., H. Xie, P. Mäkelä, S. Akiyama, S. Yashiro, M. L. Kaiser, R. A. Howard, and J.-L. Bougeret (2010), Interplanetary shocks lacking type II radio bursts, *Astrophys. J.*, *710*, 1111, doi:10.1088/0004-637X/710/2/1111.

Heppner, J. P., M. Sugiura, T. L. Skillman, B. G. Ledley, and M. Campbell (1967), OGO-A magnetic field observations, *J. Geophys. Res.*, *72*, 5417–5471.

Hoppe, M. M., and C. T. Russell (1983), Plasma rest frame frequencies and polarizations of the low-frequency upstream waves ISEE 1 and 2 observations, *J. Geophys. Res.*, *88*, 2021–2028.

Hoppe, M. M., C. T. Russell, I. A. Frank, T. E. Eastman, and E. W. Greenstadt (1981), Upstream hydromagnetic waves and their association with backstreaming ion populations ISEE 1 and 2 observation, *J. Geophys. Res.*, *86*, 4471–4492.

Hoppe, M. M., C. T. Russell, T. E. Eastman, and L. A. Frank (1982), Characteristics of the ULF waves associated with upstream ion beams, *J. Geophys. Res.*, *87*, 643–650.

Jian, L. K., C. T. Russell, J. G. Luhmann, A. B. Galvin, and P. J. MacNeice (2009a), Multi-spacecraft observations: Stream interactions and associated structures, *Sol. Phys.*, *259*, 345–360, doi:10.1007/s11207-009-9445-3.

Jian, L. K., C. T. Russell, J. G. Luhmann, R. J. Strangeway, J. S. Leisner, and B. A. Galvin (2009b), Ion cyclotron waves in the solar wind observed by STEREO near 1 AU, *Astrophys. J.*, *701*, L105, doi:10.1088/0004-637X/701/2/L105.

Jian, L. K., C. T. Russell, and J. G. Luhmann (2011), Comparing solar minimum 23/24 with historical solar wind records at 1 AU, *Sol. Phys.*, *274*, 321–344, doi:10.1007/s11207-011-9737-2.

Krauss-Varban, D., Y. Li, and J. G. Luhmann (2008), Particle acceleration and transport in the heliosphere and beyond, *AIP Conf. Proc.*, *1039*, 307–313.

Le, G., and C. T. Russell (1990), A study of the coherence length of ULF waves in the Earth's foreshock, *J. Geophys. Res.*, *95*, 10,703–10,706.

Le, G., C. T. Russell, and D. S. Orlowski (1993), Coherence lengths of upstream ULF waves: Dual ISEE observations, *Geophys. Res. Lett.*, *20*, 1755–1758.

Luhmann, J. G., et al. (2008a), IMPACT: Science goals and firsts with STEREO, *Adv. Sp. Res.*, *36*(8), 1534–1543, doi:10.1016/j.asr.2005.03.033.

Luhmann, J. G., et al. (2008b), STEREO IMPACT investigation goals, measurements, and data products overview, *Space Sci. Rev.*, *136*, 117–184, doi:10.1007/s11214-007-9170-x.

Mellott, M. M., and E. W. Greenstadt (1984), The structure of oblique subcritical bow shocks: ISEE 1 and 2 observations, *J. Geophys. Res.*, *89*, 2151–2161.

Ofman, L., M. Balikhin, C. T. Russell, and M. Gedalin (2009), Collisionless relaxation of ion distributions downstream of laminar quasi-perpendicular shocks, *J. Geophys. Res.*, *114*, A09106, doi:10.1029/2009JA014365.

Orlowski, D. S., and C. T. Russell (1991), ULF waves upstream of the Venus bow shock: Properties of one-hertz waves, *J. Geophys. Res.*, *96*, 11,271–11,282.

Orlowski, D. S., and C. T. Russell (1995), Comparison of properties of upstream whistlers at different planets, *Adv. Space Res.*, *16*, 137–141.

Orlowski, D. S., G. K. Crawford, and C. T. Russell (1990), Upstream waves at Mercury, Venus and Earth: Coparison of the properties of one hertz waves, *Geophys. Res. Lett.*, *17*, 2293–2296.

Orlowski, D. S., C. T. Russell, and R. P. Lepping (1992), Wave phenomena in the upstream regio of Saturn, *J. Geophys. Res.*, *97*, 19,187–19,199.

Orlowski, D. S., C. T. Russell, D. Krauss-Varban, N. Omidi, and M. F. Thomsen (1995), Damping and spectral formation of upstream whistlers, *J. Geophys. Res.*, *100*, 17,117–17,128.

Richardson, I. G., and V. G. Cane (2004), The fraction of interplanetary coronal mass ejections that are magnetic clouds: Evidence for a solar cycle variation, *Geophys. Res. Lett.*, *31*, L18804, doi:10.1029/2004GL020958.

Rouillard, A. P., et al. (2011), Interpreting the properties of solar energetic particle events by using combined imaging and modeling of interplanetary shocks, *Astrophys. J.*, *735*, 7, doi:10.1088/0004-637X/735/1/7.

Russell, C. T. (2007), Upstream whistler-mode waves at planetary bow shocks: A brief review, *J. Atmos. Sol. Terr. Phys.*, *69*, 1739.

Russell, C. T., C. R. Chappell, M. D. Montgomery, M. Neugebauer, and F. L. Scare (1971), Ogo 5 observations of the polar cusp on November 1, 1968, *J. Geophys. Res.*, *76*, 6743–6764.

Russell, C. T., et al. (1983), Multiple spacecraft observations of interpanetary bow shocks: Characteristics of the upstream ULF turbulence, in *Solar Wind Five*, *NASA Conf. Publ. Ser.*, vol. 2280, edited by M. Neugebauer, pp. 385–400, Natl.Aeronaut. and Space Admin., Washington, D. C.

Russell, C. T., L. K. Jian, X. Blanco-Cano, and J. G.Luhmann (2009), STEREO observations of upstream and downstream waves at low Mach number shocks, *Geophys. Res. Lett.*, *36*, L03106, doi:10.1029/2008GL036991.

Scholer, M. (1993), Upstream waves, shocklets, Schort large-amplitude magnetic structures an the cyclic behavior of oblique quasi-parallel collisionless shocks, *J. Geophys. Res.*, *98*, 47–57.

Schwartz, S. J. (1991), Magnetic field structures ad related phenomena at quasi-parallel shocks, *Adv. Space. Res.*, *11*(9), 231–240.

Schwartz, S. J., and D. Burgess (1991), Quasi-parallel shocks: A patchwork of three-dimensional structures, *Geophys. Res. Lett.*, *18*, 373–376.

Schwartz, S. J., D. Burgess, W. P. Wilkinson, R. L. Kessel, M. Dunlop, and H. Luhr (1992), Observations of short large-amplitude magnetic structures at a quasi-parallel shock, *J. Geophys. Res.*, *97*, 4209–4227.

Tsurutani, B. T., E. J. Smith, and D. E. Jones (1983), Waves observed upstream of interplanetary shocks, *J. Geophys. Res.*, *88*(A7), 5645–5656.

Wilson, L. B., III, C. A. Cattell, P. J. Kellogg, K. Goetz, K. Kersten, J. C. Kasper, A. Szabo, and K. Meziane (2009), Low-frequency whistler waves and shocklets observed at quasi-perpendicular interplanetary shocks, *J. Geophys. Res.*, *114*, A10106, doi:10.1029/2009JA014376.